Invited Review

Extended Phase Graphs: Dephasing, RF Pulses, and Echoes - Pure and Simple

Matthias Weigel, PhD[1,2]*

The extended phase graph (EPG) concept represents a powerful tool for depicting and understanding the magnetization response of a broad variety of MR sequences. EPGs focus on echo generation as well as on classification and use a Fourier based magnetization description in terms of "configurations states". The effect of gradients, radiofrequency (RF) pulses, relaxation, and motion phenomena during the MR sequence is characterized as the action of a few matrix operations on these configuration states. Thus, the EPG method allows for fast and precise quantitation of echo intensities even if several gradients and RF pulses are applied. EPG diagrams aid in the comprehension of different types of echoes and their corresponding echo time. Despite its several benefits in regard to a large number of problems and issues, researchers and users still often refrain from applying EPGs. It seems that "phase graphing" is still seen as a kind of "magic." The present review investigates the foundation of EPGs and sheds light on prerequisites for adding more advanced phenomena such as diffusion. The links between diagrams and calculations are discussed. A further focus is on limitations and simplifications as well recent extensions within the EPG concept. To make the review complete, representative software for EPG coding is provided.

Key Words: extended phase graph; phase graph; Fourier space; dephasing; configuration states; partitioning

J. Magn. Reson. Imaging 2015;41:266–295.
© 2014 Wiley Periodicals, Inc.

THE MAIN CHALLENGE: UNDERSTANDING ECHO GENERATION

Modern MRI and MR spectroscopy (MRS) sequences use gradients and radiofrequency (RF) pulses abundantly. Figure 1a depicts a still simple example of a multi spin echo sequence based on the Carr-Purcell-Meiboom-Gill (CPMG) scheme (1–3). The CPMG scheme is the basis for the commonly used MR imaging sequence known as turbo spin echo (TSE), fast spin echo (FSE), or rapid acquisition with relaxation enhancement (RARE) (4).

The general magnetization response to this CPMG sequence was simulated using the rotation operator algorithm (ROA) (5). The ROA represents the direct algorithmic conversion of the Bloch equation (6) into rotations of classical magnetization vectors (isochromats). Rotations around the z-axis by the phase angle φ represent dephasing; rotations around the x-axis by the flip angle α depict each RF pulse. RF pulses are commonly treated as instantaneous rotations (hard pulse approximation). Then, the rotation matrices

$$\mathbf{R}_x(\alpha) = \begin{pmatrix} 1 & 0 & 0 \\ 0 & \cos\alpha & -\sin\alpha \\ 0 & \sin\alpha & \cos\alpha \end{pmatrix} \quad [1]$$

and

$$\mathbf{R}_z(\varphi) = \begin{pmatrix} \cos\varphi & -\sin\varphi & 0 \\ \sin\varphi & \cos\varphi & 0 \\ 0 & 0 & 1 \end{pmatrix} \quad [2]$$

depict the effect of RF pulses and dephasing on an isochromat $(M_x, M_y, M_z)^T$. To get a correct estimate of the "real" magnetization response to a given MR sequence, a whole ensemble of isochromats, each having a different dephasing angle φ, has to be simulated. Figure 1b–d depicts the resulting magnetization response for different (so far unknown) points of time.

A general RF pulse with azimuthal phase Φ relative to the x-axis can be described using the rotation matrix composition $\mathbf{R}_\Phi(\alpha) = \mathbf{R}_z(\Phi) \, \mathbf{R}_x(\alpha) \, \mathbf{R}_z(-\Phi)$, which leads the general rotation back to a rotation around x (1,2).

Figure 1 demonstrates that the ROA is well suited for graphical simulations of the Bloch equation (5); however, it is less practical for the quantitation of echo intensities. To attain the necessary accuracy, the evolution of typically thousands of isochromats has to be determined over time, i.e., by solving the Bloch equation. Finally, the vector sum of all isochromats has to be calculated. This is neither computationally efficient nor an exact solution for the echo intensities.

[1]Department of Radiology, Medical Physics, University Medical Center Freiburg, Freiburg, Germany.

[2]Radiological Physics, University of Basel Hospital, Basel, Switzerland.

*Address reprint requests to: M.W., Radiological Physics, University of Basel Hospital, Petersgraben 4, 4031 Basel, Switzerland. E-mail: matthias.weigel@usb.ch
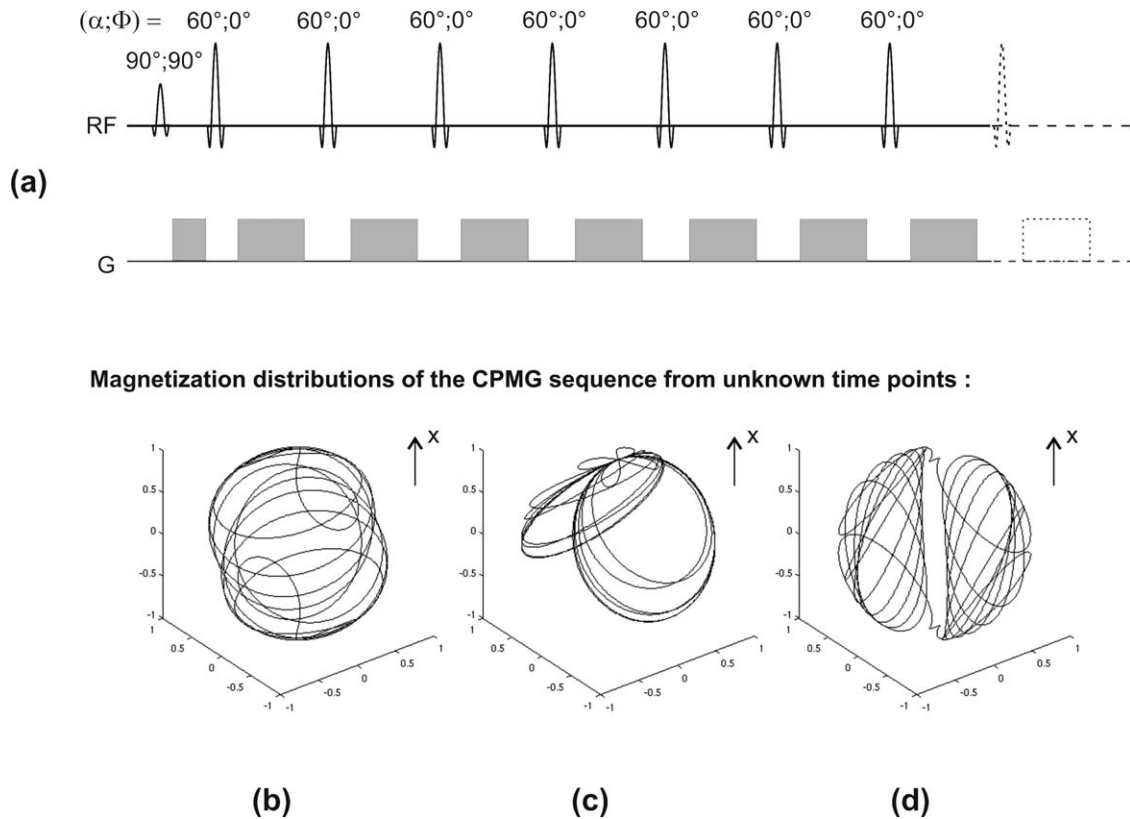
Figure 1. a: Example of a CPMG sequence with constant flip angle $\alpha = 60^{\circ}$ refocusing pulses. The magnetization response was simulated using the Bloch equation with 5000 isochromats. **b–d:** Three screenshots of the resulting magnetization response in position space are shown for different unknown points of time. It is rather unclear whether one or more screenshots represent an echo and, if so, what type of echo(es) with which intensity are observed.

Also, intuitive insight remains very limited: It is difficult to *read* the magnetization response from the sequence diagram or graphical Bloch simulation in Figure 1. Important questions that may arise include: When do echoes occur? If an echo occurs what type is it? Spin echo (SE)? Stimulated echo (STE)? Is there in fact a general way to identify types of echoes (echo *classification*)?

In the present context an *echo* means a nonvanishing macroscopic transverse magnetization component that develops during free precession. In reference to Figure 1c, a close look still reveals that all isochromats have nonnegative x-components. This asymmetry in isochromat distribution with respect to the y-z plane clearly hints at an echo. Using a similar argument in the opposite way, Figures 1b and d probably display fully dephased magnetization. However, there does not appear to be much hope of deducing further information from Figure 1b–d about echo intensity, time point, etc.

Extended phase graphs (EPGs) (7–19) represent a powerful and elegant tool to answer the questions put forth above. In the following, the foundations of the EPG concept will be analyzed and explained in both a pictorial and a quantitative way. Recipes how to properly add effects of relaxation, coherent motion, or diffusion are provided. There is an additional focus on graphical representation, on a few common stumbling blocks, and also on the limita-

tions and simplifications involved in this framework. The work is completed by representative examples and information on the availability of dedicated software.

Describing Dephased Magnetization in an Efficient Way

Dephasing represents an important phenomenon in magnetic resonance. Particularly gradients — which realize spatial encoding, spoiler and crusher gradients, introduce motion sensitivity for diffusion and flow, etc. — cause inevitable dephasing. Thus, most of the time the isochromat ensemble ("spin system") is in a state of strong dephasing as shown in Figure 2. Coherence only occurs during the short period of echo generation. However, dealing with dephased magnetization in position space is an extensive task (Fig. 2), because for each isochromat the Bloch equation has to be solved.

For an improved description of dephasing it makes sense to recall the basic effect of a gradient. First, the focus will be on transverse magnetization, i.e., coherent transverse magnetization after excitation as demonstrated in Figure 3: Using the rotating reference frame introduced by Rabi et al (20), the constant gradient G introduces a linearly position-dependent off-resonance Larmor frequency ω along its axis. A right-handed helix of isochromat endpoints evolves in
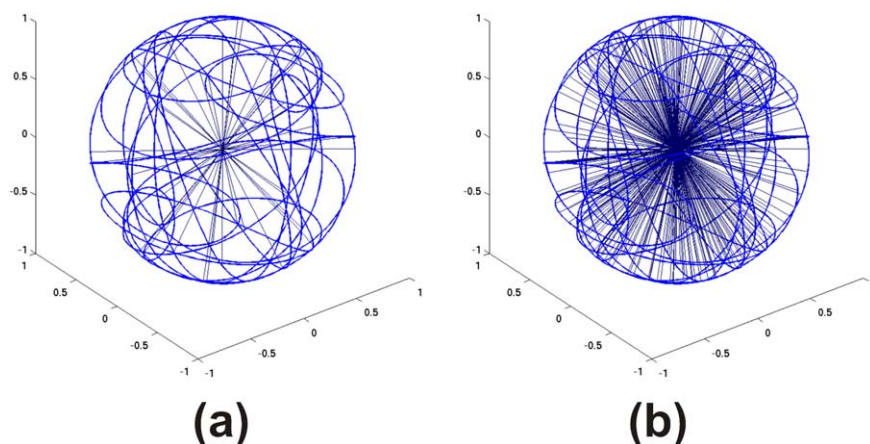
Figure 2. Example of the configuration of a strongly dephased isochromat ensemble. To get an idea of the "exact ensemble configuration," interpolation between thousands of isochromat supporting points had to be performed (light blue color). Drawing a fraction of these isochromats (dark blue color) demonstrates how much information content is needed to properly describe a dephased isochromat system after several applied RF pulses. 50 (**a**) and 500 (**b**) selected isochromats are shown. [Color figure can be viewed in the online issue, which is available at wileyonlinelibrary.com.]

space, if the gradient is presumed to be along the z-axis (Fig. 3).[1]

In the following, all pictorial sketches of isochromat helices (transverse magnetization) will presume a gradient in the z-direction. The reader should note that this assumption is without loss of generality for the later results, that magnetization distributions of spatial harmonics (helices) will evolve. Neither does this assumption have any influence on the final quantitative results. It is merely for the sake of improved visualization and pictorial understanding of what a gradient's effect is.

The longer the gradient is turned on (Fig. 3), the more turns the helix will have, which is equivalent to higher spatial frequency or smaller wave length. To find a more compact representation of such dephasing, a closer look at such a helix and a given single isochromat is provided in Figures 4a and b: The equation of motion for a single isochromat with magnitude $M = |\mathbf{M}|$ at off-center position $\mathbf{r}$ equals

$$M_x(\mathbf{r}) = M \cos\left(\gamma \mathbf{r} \int_0^t \mathbf{G}(t') \ dt'\right) = M \cos(\mathbf{kr}) \quad [3a]$$

$$M_y(\mathbf{r}) = M \sin\left(\gamma \mathbf{r} \int_0^t \mathbf{G}(t') \ dt'\right) = M \sin(\mathbf{kr}) \quad . \quad [3b]$$

Equations (3a) and (3b) used the phase angle $\phi(\mathbf{r}) = \int_0^t \gamma \mathbf{G}(t')\mathbf{r} \ dt'$ and is defined at a given time t; thus, there is no explicit time dependence in the equations given. The angular wave vector

$$\mathbf{k}(t) = \gamma \int_0^t \mathbf{G}(t') \ dt' \quad [4]$$

was introduced (13–16,18), which describes the helix's spatial frequency over time, its inverse times 2π being the pitch λ of the helix. Therefore, $\mathbf{k}$ represents a quantitative measure for dephasing ("order of dephasing") and is already well-known from the popular k-space concept (21,22).

The dephasing effect of gradients generates time-dependent harmonic (sine and cosine) magnetization

components along the spatial axes (Eqs. (3a) and (3b)), which correspond to the helices in Figures 3 and 4 for a z-gradient. A change of basis from real M_x, M_y to the complex magnetization components (7)

$$M_+(\mathbf{r}) = M_x(\mathbf{r}) + iM_y(\mathbf{r}) = M \ e^{i\phi(\mathbf{r})} = M \ e^{i\mathbf{kr}} = (M_-)^* \quad [5a]$$

$$M_-(\mathbf{r}) = M_x(\mathbf{r}) - iM_y(\mathbf{r}) = M \ e^{-i\phi(\mathbf{r})} = M \ e^{-i\mathbf{kr}} = (M_+)^* \quad [5b]$$

allows a simplified description of transverse magnetization (Fig. 4c), thereby avoiding the distinction between x and y magnetization components that have mutual magnetization exchange over time. The symbol "*" denotes the complex conjugate operation; $i = \sqrt{-1}$ is the imaginary unit.

The reader should note that M_- directly corresponds to that magnetization if M_+ is flipped ("refocused") by a 180° RF pulse around the x-axis (Eqs. (5a) and (5b); Fig. 4c). From a notational point of view, the fact that the effect of a 180° RF pulse around the x-axis can be depicted by a single complex conjugate operation $(M_+)^* = M_-$ is of highly practical value within the field of MR. This property was already reported by Jaynes and Woessner (7,8) and will be of high importance throughout the text.

Neglecting M_- for the moment, the sum of all isochromats (i.e., the helix, Eq. (5a) and Fig. 4a) along the gradient's direction represents the net magnetization. In the continuous limit this corresponds to the integral $\int M \ e^{i\mathbf{kr}} d^3r$. Considering the integral as being evaluated over a macroscopically large sample (sub)volume V (c.f. chapter "Extensions, Limitations and Software Coding"), where, generally, various helices of different spatial frequency, wave vector or dephasing order $\mathbf{k}$ will be present, leads to the relation:

$$\tilde{F}_+(\mathbf{k}) = \int_V \left(M_x(\mathbf{r}) + iM_y(\mathbf{r})\right) \ e^{-i\mathbf{kr}} \ d^3r = \int_V M_+(\mathbf{r}) \ e^{-i\mathbf{kr}} \ d^3r$$

$$\Longleftrightarrow M_x(\mathbf{r}) + iM_y(\mathbf{r}) = M_+(\mathbf{r}) = \int_V \tilde{F}_+(\mathbf{k}) \ e^{i\mathbf{kr}} d^3k \quad . \quad [6]$$

Equation (6) interprets transverse magnetization as a sum of complex spatial harmonics (helices) with different wave vectors $\mathbf{k}$. However, Eq. (6) is nothing else than the Fourier decomposition of $M_+(\mathbf{r})$. Therefore, the Fourier transform $\tilde{F}_+(\mathbf{k})$ depicts for each helix of

[1]CONVENTION: A positive gradient will lead to a higher Larmor frequency on the positive side of the right-handed spatial coordinate system, which leads to a counterclockwise precessing isochromat, which corresponds to a mathematically positive sense of rotation and precession. Thus, a right-handed helix evolves due to dephasing with a positive gradient.

Gradient G
(z-direction presumed)

Gradient

G–

0–

Time *t*

Figure 3. Visualization of a z gradient's dephasing effect on initially coherent transverse magnetization. The lowest isochromat is on-resonant ($\omega = 0$) at the "isocenter"; the off-resonance frequency increases linearly with the distance from the imaginary isocenter. The 40 representative isochromats begin to form a helicoid and their endpoints a helix around the z-axis, as emphasized by the rainbow colored tube. With time, the right-handed helix turns more and more and its corresponding pitch decreases. For reasons of improved visualization, a gradient along the z-axis was presumed and its negative part omitted (c.f. text).
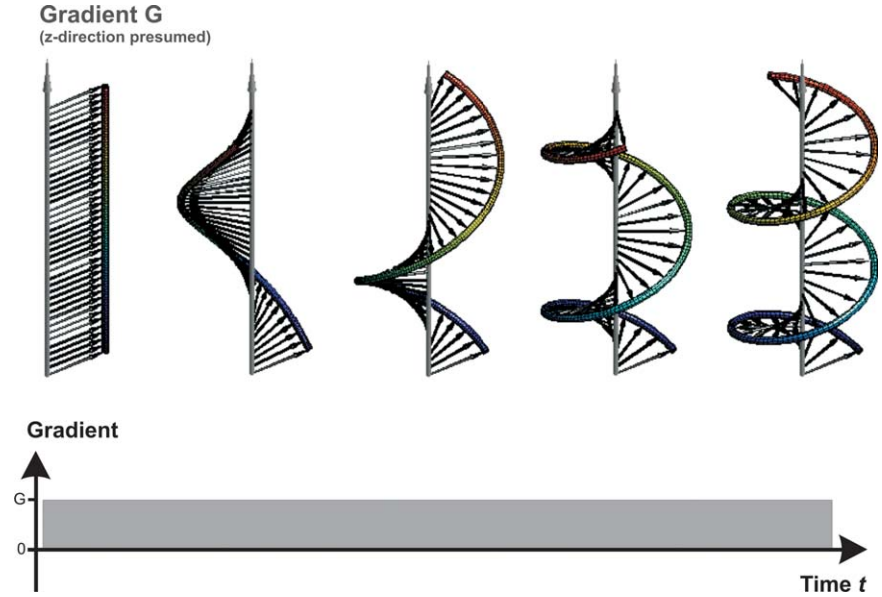
wave vector **k** its amplitude (radius) and its phase (phase angle in the x′-y′-plane) in Eq. (6). Any possible scaling factor of the inverse or forward Fourier transform was included within M_+ or $\tilde{F}_+$ in Eq. (6).

The tilde notation is meant to emphasize that $\tilde{F}_+(\mathbf{k})$ is defined in Fourier space and provides Fourier components. Former publications used F at the same time for both Fourier (Eq. (6)) and non-Fourier based magnetization components, i.e., F and F^* instead of M_+ and M_- (8,11,15,17). Or, on the contrary, authors also used M_+ and M_- notations for the Fourier space (8,11,15,17). This should be avoided by all means, because it leads to ambiguities and is prone to error. In this manuscript, M always refers to magnetization components in position space; F is always connected to Fourier space.

Coming back to the helix-dephasing illustration in Figure 3, Figure 5 pin-points the elegance and efficiency of the Fourier approach: Magnetization is interpreted in terms of "*configuration states*" (11) that are directly linked to the dephasing coordinate **k**. Particu-

larly, a simple change of **k** means the corresponding change of dephasing of the whole isochromat ensemble's transverse magnetization $\tilde{F}_+(\mathbf{k})$ (10–16,18,23,24). This approach by means of configuration states is so efficient because we directly describe the gradient dephasing in a system of reference, which the gradients in a manner of speaking "generate themselves": a sum of helices of isochromats.
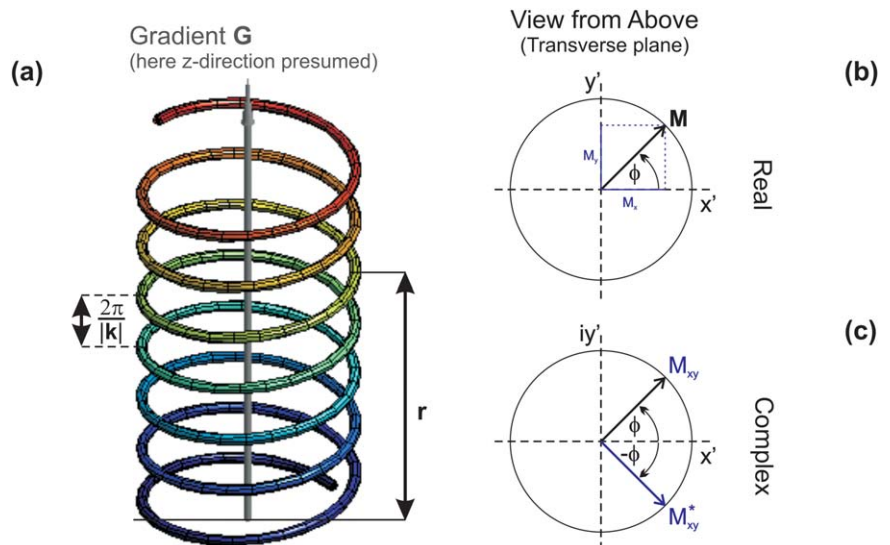
Configuration states are also termed phase states, coherences, base states, partition states, etc. in the literature. They represent the first of two key concepts within the EPG calculus. Now, the second key concept will be used to account for the effect of RF pulses on magnetization components and configuration states in particular.

Action of RF Pulses

Partition State Method

MR experiments consist of two basic probes: (i) gradients and (ii) RF pulses. After the first significant

(a) Gradient **G**
(here z-direction presumed)

View from Above **(b)**
(Transverse plane)

y′
M
M_y
ϕ
M_x
x′

Real

iy′ **(c)**
M_{xy}
ϕ
x′
ϕ
M_{xy}^*

Complex

Figure 4. a: Example of an evolved helix of isochromats with the pitch $2\pi/|\mathbf{k}|$ along the z-axis. **b:** At a distance **r** from the isocenter along the gradient $\mathbf{G_z}$, the equation of motion of the respective transverse magnetization vector **M** is analyzed in further detail. **c:** The change to a complex representation of transverse magnetization leads to simplification and new physical insights as described in the text.
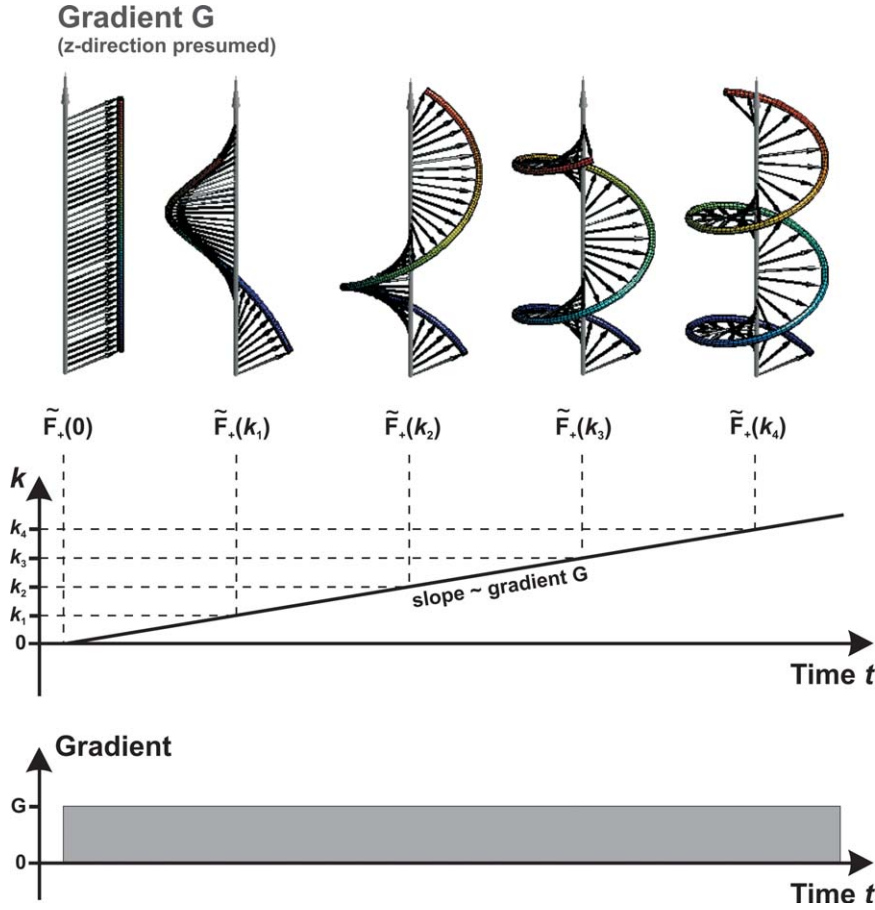
Gradient G
(z-direction presumed)

$$\tilde{F}_+(0) \qquad \tilde{F}_+(k_1) \qquad \tilde{F}_+(k_2) \qquad \tilde{F}_+(k_3) \qquad \tilde{F}_+(k_4)$$

Figure 5. In reference to Figure 3, the dephasing effect of gradient **G** (bottom) on transverse magnetization is quantified in terms of k (middle, here a 1D scalar), which increases linearly with time due to the constant (background) gradient. Directly connected to k is the corresponding helix $\tilde{F}_+(k)$, called configuration state, which exactly depicts the configuration of transverse magnetization present at that time. [Color figure can be viewed in the online issue, which is available at wileyonlinelibrary.com.]

improvement in characterizing the effect of gradients on isochromat ensembles in terms of the configuration states (last chapter), describing the effect of RF pulses on magnetization components shall be improved now. This search leads back to the historical beginnings of "phase graphing," which was originally published as the *partition state method* (8,9). The partition state method still investigated magnetization in position space (Eqs. (5a) and (5b)). In the following, the basic theory of and results from the partition state method are discussed and then combined with the concept of configuration states to obtain the *extended phase graphs*, the way in which phase graphs are interpreted nowadays.

The rotation matrices $\mathbf{R_x}$ and $\mathbf{R_z}$ used in the ROA approach from Eqs. (1) and (2) are solved for the complex transverse magnetization basis (8,9,11). A fast and elegant change between the two reference systems is achieved by a pair of similarity (**S** and $\mathbf{S^{-1}}$) or unitary (**U** and $\mathbf{U^{-1}}$) transformation matrices:

$$\begin{pmatrix} M_x \\ M_y \\ M_z \end{pmatrix} \underset{\mathbf{S^{-1} \, or \, U^{-1}}}{\overset{\mathbf{S \, or \, U}}{\rightleftharpoons}} \begin{bmatrix} \rho\,M_+ \\ \rho\,M_- \\ M_z \end{bmatrix} \quad \rho : \text{Scaling factor for basis.} \quad [7]$$

The exponent "−1" denotes the inverse transformation matrix. The definition in this text is that vectors and matrices referring to the real reference system are put in parentheses, whereas for the complex reference system brackets are used.

Compared with the similarity transformation for which $\rho = 1$ in Eq. (7), the unitary transformation for which $\rho = 1/\sqrt{2}$ preserves the original norm of the magnetization vectors, which is $|\mathbf{M}| = \sqrt{M_x^2 + M_y^2 + M_z^2}$. This can be easily seen considering that both M_+ and M_- contain M_x and M_y, but M_z occurs only once. Directly proving it is left as an exercise for the reader.

Besides preserving the norm, the advantage of the unitary transformation is that it also preserves a rotation matrix as a rotation matrix, and the matrices **U** and $\mathbf{U^{-1}}$ are a kind of "symmetrically defined":

$$\mathbf{U} = \frac{1}{\sqrt{2}} \begin{pmatrix} 1 & +i & 0 \\ 1 & -i & 0 \\ 0 & 0 & \sqrt{2} \end{pmatrix} \qquad [8a]$$

$$\mathbf{U^{-1}} = \frac{1}{\sqrt{2}} \begin{bmatrix} 1 & 1 & 0 \\ -i & +i & 0 \\ 0 & 0 & \sqrt{2} \end{bmatrix}. \qquad [8b]$$

For unitary matrices it is $\mathbf{UU^\dagger} = \mathbf{UU^{-1}} = 1$, which makes it simple to find the corresponding inverse as $\mathbf{U^{-1}} = \mathbf{U^\dagger}$. The symbol "$\dagger$" signifies the Hermitian conjugate of vectors and matrices. The similarity transformation matrices are defined as

$$\mathbf{S} = \begin{pmatrix} 1 & +i & 0 \\ 1 & -i & 0 \\ 0 & 0 & 1 \end{pmatrix} \qquad [9a]$$

$$\mathbf{S}^{-1} = \frac{1}{2}\begin{bmatrix} 1 & 1 & 0 \\ -i & +i & 0 \\ 0 & 0 & 2 \end{bmatrix}. \qquad [9b]$$

In some situations, such as in the investigation of transient phase behavior of steady state sequences as performed by Ganter (25,26), the unitary transformation in Eqs. (8a) and (8b) may be more convenient; however, its disadvantage is that the scaling factor $\rho = 1/\sqrt{2}$ occurs in some components of all further vectors and operator matrices. Thus, the similarity transformation will be used further on for practical reasons. This is in accordance with the vast majority of publications which use Eqs. (9) directly or indirectly (7–18,23,24,27–29). If the reader should be interested in or in need of the more concise unitary transformation, he or she has to replace all the following $\mathbf{S}$ and $\mathbf{S}^{-1}$ matrices with $\mathbf{U}$ and $\mathbf{U}^{-1}$ matrices, respectively.

According to linear algebra, the new RF pulse and dephasing matrices are defined by means of $\mathbf{T} = \mathbf{S}\,\mathbf{R}\,\mathbf{S}^{-1}$, thence (8,9,16)

$$\mathbf{T_x}(\alpha) = \begin{bmatrix} \cos^2\frac{\alpha}{2} & \sin^2\frac{\alpha}{2} & -i\,\sin\alpha \\[2mm] \sin^2\frac{\alpha}{2} & \cos^2\frac{\alpha}{2} & +i\,\sin\alpha \\[2mm] -\frac{i}{2}\,\sin\alpha & +\frac{i}{2}\,\sin\alpha & \cos\alpha \end{bmatrix} \qquad [10]$$

and

$$\mathbf{T_z}(\varphi) = \begin{bmatrix} e^{+i\varphi} & 0 & 0 \\ 0 & e^{-i\varphi} & 0 \\ 0 & 0 & 1 \end{bmatrix}. \qquad [11]$$

For Eq. (10) the trigonometric identities $\frac{1}{2}\,(1+\cos\alpha) = \cos^2\frac{\alpha}{2}$ and $\frac{1}{2}\,(1-\cos\alpha) = \sin^2\frac{\alpha}{2}$ were used, because these results allow a better intuitive insight. $\mathbf{T_x}$ does not have the property of a rotation matrix anymore because a nonunitary transformation was used. This fact was already noted by Hennig (11).

Combining Eqs. (10) and (11) by means of $\mathbf{T_\Phi}(\alpha) = \mathbf{T_z}(\Phi)\,\mathbf{T_x}(\alpha)\,\mathbf{T_z}(-\Phi)$ gives the solution for general RF pulses with initial RF phase angles of $\Phi \neq 0$, i.e., not rotating around the x-axis, which act on a complex magnetization vector (16)

$$\begin{bmatrix} M_+ \\ M_- \\ M_z \end{bmatrix}^+ = \begin{bmatrix} \cos^2\frac{\alpha}{2} & e^{2i\Phi}\sin^2\frac{\alpha}{2} & -ie^{i\Phi}\sin\alpha \\[2mm] e^{-2i\Phi}\sin^2\frac{\alpha}{2} & \cos^2\frac{\alpha}{2} & ie^{-i\Phi}\sin\alpha \\[2mm] -\frac{i}{2}e^{-i\Phi}\sin\alpha & \frac{i}{2}e^{i\Phi}\sin\alpha & \cos\alpha \end{bmatrix}$$
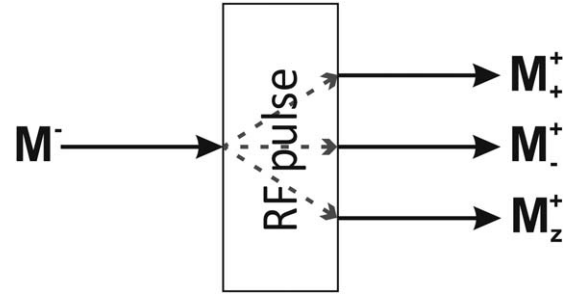$$\cdot \begin{bmatrix} M_+ \\ M_- \\ M_z \end{bmatrix}^-. \qquad [12]$$

Figure 6. Partitioning effect of an arbitrary RF pulse as described by Kaiser et al (9) in the layout K. Scheffler presented several years ago: An isochromat M^- before the RF pulse is split into three parts in dependence on the flip angle α: One part is dephasing transverse magnetization M_+, one part is rephasing transverse magnetization M_-, and one part is a longitudinal component M_z. From the author's experience, it should be said that partitioning is not just a "mathematical trick"; it is a wise choice of the system of reference that explains exactly what we see for low flip angles α: They indeed refocus transverse magnetization but in an imperfect way, and they rotate magnetization into the longitudinal direction.

The exponents "−" and "+" signify the common notation of magnetization "before" and "after" the RF pulse was applied (11,13,15,17,18).

Equation (12) has extraordinary implications for the field of NMR and represents the essence of phase graph concepts in general (8,9): After an RF pulse has been applied, magnetization behaves like a composition or superposition of three different parts: (i) Dephasing transverse magnetization (M_+ component); (ii) Rephasing transverse magnetization that can produce an echo (M_- component); (iii) Longitudinal magnetization (M_z component).

This observation, known as the *Woessner decomposition*, was proven by Woessner, by means of the Schrödinger equation, to be true for spin $1/2$ particles (8). Kaiser et al introduced the term *partitioning effect of an RF pulse* (9); the term is frequently found in the literature or heard in oral presentations. Figure 6 illustrates this partitioning in a graphical way.

In detail, the Woessner decomposition means that from the perspective of initial transverse M_+ magnetization, the first part remains unaffected dephasing transverse magnetization ("0° pulse"), the second part is refocused ("180° pulse") and the third part becomes longitudinal magnetization ("90° pulse") (8,9). From the perspective of initial longitudinal M_z magnetization, the first part becomes dephasing transverse magnetization, the second part becomes rephasing transverse magnetization and the third part stays unaffected in the longitudinal direction (8,9). However, if the investigated RF pulse is the first in the sequence, no rephasing magnetization component is generated. In all cases the fractions of the three different parts depend on the flip angle α.

Here, the reader should note that descriptions like "0° pulse, 90° pulse, 180° pulse" are nice mnemonics but are only true from the perspective of transverse magnetization; otherwise they are nonsense — a 180° pulse would invert longitudinal z-magnetization, for instance.

The observation of the partitioning effect is of such great value because it explains with a simple model that lower flip angles lead to less refocusing of transverse magnetization (spin echoes) and that, generally, also longitudinal magnetization can take part in the formation of echoes (stimulated echoes). Additionally, a closer look at Eq. (12) reveals that no phase component has any influence on the quantitative partitioning; it solely depends on the flip angle α. The RF phase Φ is only present in complex phase terms and the phase of the initial magnetization is not present at all. It is just contained within the initial magnetization vector, right side of Eq. (12). This observation makes sense because the partitioning should definitely not depend on the rotation of our coordinate system around the z-axis: the choice of the x-axis where the RF pulse rotates around is arbitrary. Furthermore, it must be said that we reside in the rotating reference frame anyway (20). So the phase of the initial magnetization and also of the RF pulse will only influence the phase of the resulting magnetization, including the generated spin and stimulated echoes. This will become more apparent later (c.f. Eqs. (16)).

A sequence of RF pulses splits successively all present partitions into three further partitions each (Eq. (12), Fig. 6). This whole description is called the *partition state method* (8,9) and together with dedicated graphical diagrams it represents the original phase graph approach. In its full detail, the partition state method already allows the characterization of echo generation, the calculation of echo times and the quantitation of the corresponding echo intensities. Although obviously powerful, it must be said that the partition state method starts with one representative isochromat/magnetization vector of a defined off-resonance frequency. This is split according to Eq. (12) due to RF pulses. Thus, effects like the phase storage in the z-direction or diffusion are possible to model but nevertheless hard to understand, because these are effects of the whole isochromat ensemble. Thus, by combining the two key concepts of RF pulse partitioning and Fourier based configuration states, a phase graph approach that depicts the evolution of a complete isochromat ensemble is created. This framework is called the extended phase graph (EPG) concept.

Extended Phase Graphs

The key concept of configuration states was previously based on the Fourier decomposition of transverse magnetization. Now, the full complex system of reference $[M_+, M_-, M_z]^T$ is expressed by means of Fourier decompositions and transforms (10–19,24–26,28):

$$\tilde{F}_+(\mathbf{k}) = \int_V \left(M_x(\mathbf{r}) + i M_y(\mathbf{r}) \right) e^{-i\mathbf{kr}} d^3r = \int_V M_+(\mathbf{r}) e^{-i\mathbf{kr}} d^3r$$
$$\Longleftrightarrow M_x(\mathbf{r}) + i M_y(\mathbf{r}) = M_+(\mathbf{r}) = \int_V \tilde{F}_+(\mathbf{k}) e^{i\mathbf{kr}} d^3k,$$

[13a]

$$\tilde{F}_-(\mathbf{k}) = \int_V \left(M_x(\mathbf{r}) - i M_y(\mathbf{r}) \right) e^{-i\mathbf{kr}} d^3r = \int_V M_-(\mathbf{r}) e^{-i\mathbf{kr}} d^3r$$
$$\Longleftrightarrow M_x(\mathbf{r}) - i M_y(\mathbf{r}) = M_-(\mathbf{r}) = \int_V \tilde{F}_-(\mathbf{k}) e^{i\mathbf{kr}} d^3k,$$

[13b]

$$\tilde{Z}(\mathbf{k}) = \int_V M_z(\mathbf{r}) e^{-i\mathbf{kr}} d^3r$$
$$\Longleftrightarrow M_z(\mathbf{r}) = \int_V \tilde{Z}(\mathbf{k}) e^{i\mathbf{kr}} d^3k.$$

[13c]

Equations (13a) to (13c) closely follow the notation explained by Weigel et al to avoid ambiguities with complex conjugate operations (18). This is directly consistent with the notation of components M_+ and M_-, which were already used by Jaynes (7); and it is in close agreement with other areas of physics such as quantum mechanics.

Equations (13a) to (13c) define our new system of reference $[\tilde{F}_+, \tilde{F}_-, \tilde{Z}]^T$ using the concept of configuration states for all magnetization components M_+, M_-, and M_z. $\tilde{F}_+(k)$ denotes dephasing transverse magnetization and is already known from Eq. (6). It is based on M_+ and can be illustrated pictorially by a right-handed helix (Fig. 5). $\tilde{F}_-(-k)$ represents the pendant with reversed phase history and corresponds to a helix of opposite chirality (left-handed helix). It is based on the component M_- being the rephasing part as explained earlier by the partition state method. Thus, $\tilde{F}_-(-k)$ must represent configuration states of rephasing transverse magnetization components that are able to generate echoes.

But, the Fourier transform of M_z in Eq. (13c) may be surprising; even more surprising is the fact that a complex Fourier transform is used, because longitudinal M_z magnetization is always real-valued. Gradients cause harmonic wave patterns of transverse magnetization as denoted by $\tilde{F}_+(k)$ and $\tilde{F}_-(-k)$. From the partition state method and other fundamental physics of NMR it is known that RF pulses convert transverse into longitudinal magnetization components and vice versa. Thus, generated spatial harmonics of transverse magnetization $\tilde{F}_+(k)$ and $\tilde{F}_-(-k)$ with $k \neq 0$ are rotated into the longitudinal direction to become so called *modulated longitudinal magnetization* $\tilde{Z}(k)$. Therefore, to obtain a complete Fourier representation it just makes sense to depict longitudinal magnetization in Fourier components as well (11,13–15,18).

Another fundamental property of $[\tilde{F}_+, \tilde{F}_-, \tilde{Z}]^T$ to consider is that the change of reference system from initially three independent real magnetization components M_x, M_y, and M_z to three complex (Fourier) states $\tilde{F}_+, \tilde{F}_-, \tilde{Z}$ leads to an increase to 2*3 = 6 components. Thus, dependencies must exist to account for the new redundancy involved (11,14,15,18):

$$\left(\tilde{F}_+(\mathbf{k}) \right)^* = \tilde{F}_-(-\mathbf{k}),$$

[14a]

$$\left(\tilde{Z}(\mathbf{k}) \right)^* = \tilde{Z}(-\mathbf{k}).$$

[14b]

The relation between the dephasing $\tilde{F}_+$ and the rephasing $\tilde{F}_-$ configuration states (Eq. (14a)) often becomes important in EPG coding (c.f. chapter "Extensions, Limitations and Software Coding") and will also be discussed in the chapter "Examples for MRI Sequences."

The symmetry in the $\tilde{Z}$ states (Eq. (14b)) is the direct consequence of (complex) Fourier transforming the

real-valued magnetization. It ensures that the Fourier based longitudinal magnetization remains real. Thus, longitudinal $\tilde{Z}$ states should always be thought of as a pair of $\tilde{Z}(\mathbf{k})$ and $\tilde{Z}(-\mathbf{k})$. This corresponds to two counter-rotating circularly polarized waves or helices that represent together a linear harmonic magnetization modulation in the z-direction (11).

But why is a complex Fourier transform for M_z used at all (Eq. (13c))? This question is a bit trickier and it can be justified by three arguments that are mutually linked: First, it is a matter of consistency. All components are treated equally and, thus, a uniform Fourier representation of magnetization components is obtained. Second, it is much easier to do analytical calculations with exponential functions than with sine or cosine functions. Regarding analytical calculations, it has to be considered that Eqs. (13a) to (13c) always allow the conversion of any given magnetization constellation into a set of configuration states and vice versa at any time. And third, $\tilde{F}_+(\mathbf{k})$ and $\tilde{F}_-(-\mathbf{k})$ carry both magnitude and phase information. The phase information describes a shift of the wave pattern in space relative to the origin and this shift is not lost if transverse harmonic components are rotated into longitudinal magnetization components, becoming modulated $\tilde{Z}(\mathbf{k})$ states. So, both a phase and magnitude representation will be needed for the $\tilde{Z}(\mathbf{k})$ states as well, which makes it highly advisable to use complex Fourier components. Consequently, regarding the basis function $\tilde{Z}(\mathbf{k})$ in Eq. (13c), it would *not* be enough to use either a real-valued sine or a cosine transform to get the full information; both would be needed. Although combinations of a sine or cosine term with complex amplitudes are thinkable, this obviously leads more to confusion than to a concise and consistent representation. Thus, the reasoning leads back to the first argument of a consistent representation. For this reason, all publications after Hennig's original publications about EPGs used the full complex Fourier basis functions (14–19,24,25,28,30). The importance of possible phase storage in the longitudinal direction will be discussed in further detail further on below.

Equations (13a) to (13c) continue to use a full three-dimensional (3D) representation with 3D space and dephasing coordinates. This is essential if multiple encoding directions are to be considered simultaneously or anisotropic diffusion effects are to be investigated (18). A 1D dephasing coordinate is normally sufficient, however, for understanding the magnetization response of multi-pulse sequences. Thus, the literature almost exclusively deals with a 1D approach using the read/frequency encoding direction (10–17,19,23–29), and the same will be done here for reasons of simplicity. Thus, the vectors $\mathbf{k}$ and $\mathbf{r}$ reduce to the scalars k and r, respectively. All fundamental EPG-1D results, however, are also valid for the 3D approach. For further comments on using a full 3D approach the reader should refer to the chapter "Extensions, Limitations and Software Coding".

In the following, the effect of RF pulses on the configuration states will be investigated, i.e., combining the partition state method with the configuration theory. Thus, substituting the magnetization vectors M_+, M_-, and M_z in Eq. (12) with the Fourier transforms of Eqs. (13a) to (13c), an element-wise comparison (16,24) leads to the result how RF pulses affect the configuration states (10–19,23–26,28):

$$\begin{bmatrix} \tilde{F}_+(k) \\ \tilde{F}_-(-k) \\ \tilde{Z}(k) \end{bmatrix}^+ = \begin{bmatrix} \cos^2\frac{\propto}{2} & e^{2i\Phi}\sin^2\frac{\propto}{2} & -ie^{i\Phi}\sin\propto \\ e^{-2i\Phi}\sin^2\frac{\propto}{2} & \cos^2\frac{\propto}{2} & ie^{-i\Phi}\sin\propto \\ -\frac{i}{2}e^{-i\Phi}\sin\propto & \frac{i}{2}e^{i\Phi}\sin\propto & \cos\propto \end{bmatrix} \begin{bmatrix} \tilde{F}_+(k) \\ \tilde{F}_-(-k) \\ \tilde{Z}(k) \end{bmatrix}^-. \quad [15]$$

Indeed, the center $\mathbf{T}_\Phi(\alpha)$-matrix operator in Eq. (15) is exactly the same as in Eq. (12), because the Fourier transform is a linear transformation and $\mathbf{T}$ does not explicitly depend on k. As a result, RF pulses only mix configuration states of equal dephasing order $|k|$, i.e., $\tilde{F}_+(k)$, $\tilde{F}_-(-k)$, and $\tilde{Z}(k)$ (10–18,23–26,28), because they realize the same rotation for all states.

The last paragraphs already discussed the basic meaning of the different Fourier based states $\tilde{F}_+(k)$, $\tilde{F}_-(-k)$, and $\tilde{Z}(k)$. Now, Figure 7 pin-points the meaning of Eqs. (13a) to (13c) and (15) by means of the already known helix representations. As was noted before, longitudinal magnetization distributions have to be visualized as linear, harmonic magnetization patterns (Fig. 7), because each longitudinal helix $\tilde{Z}(k)$ has a "hidden" antisymmetric, complex conjugated partner $\tilde{Z}(-k)$, i.e., a counter-rotating helix (Eq. (14b) and Refs. (11,15,18)). For $k \neq 0$, an RF pulse exchanges or mixes fractions of magnetization among the three mutual partners with identical $|k|$ of dephasing $\tilde{F}_+(k)$ and rephasing $\tilde{F}_-(-k)$ transverse components as well as modulated $\tilde{Z}(k)$ longitudinal components. The fractions depend on the flip angle and are defined by the $\mathbf{T}_\Phi(\alpha)$-matrix operator in Eq. (15) (10–18,23–26,28). In the EPG representation, it is also said that the RF pulse exchanges populations between different configuration states, the complex-valued populations carrying magnitude and phase information. From now on, all changes of these populations of the configuration states will be performed by dedicated *operators* representing physical effects such as RF pulses, relaxation, diffusion and so on (17,18).

In Figure 7, the opportunity is also taken to link the exchange of populations between the configuration states with basic scientific MR terms such as *refocusing* or *storing*, which are also used in non-phase graph related literature. The EPG concept considerably aids in the understanding of the common MR term "storing
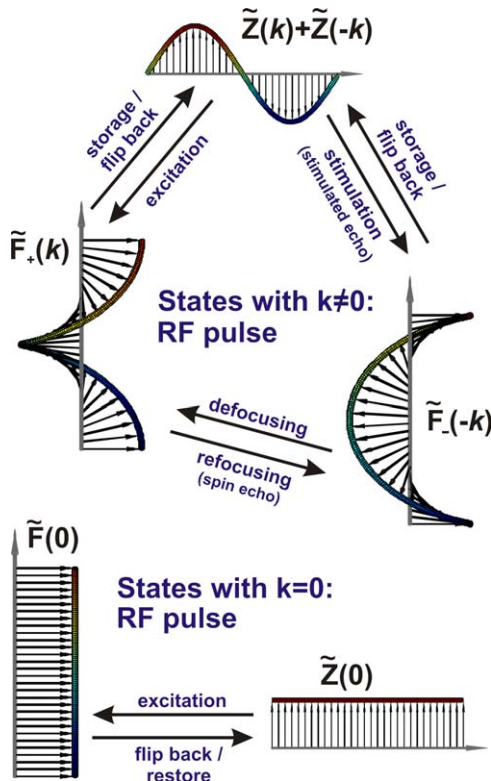
Figure 7. Graphical interpretation of an RF pulse affecting the EPG configuration states. Only the positive side from the isocenter of the helices ($\tilde{F}$ states) and linear waves ($\tilde{Z}$ states) is shown. Each RF pulse causes an exchange of magnetization between equal dephasing orders only. For $k = 0$, $\tilde{F}_+$ and $\tilde{F}_-$ are redundant states by mere complex conjugation (Eq. (14a)), thus denoted here as $\tilde{F}(0)$. Conversion from $\tilde{Z}(0)$ to $\tilde{F}(0)$ represents an FID. For $k \neq 0$, magnetization is exchanged between $\tilde{F}_+$, $\tilde{F}_-$, and $\tilde{Z}$. Particularly important is magnetization as $\tilde{F}_-$, because it represents rephasing magnetization that can generate a spin or a stimulated echo, depending on its former magnetization history. Conversion from $\tilde{F}$ to $\tilde{Z}$ is usually called "storing", but may also be seen as "flip back" depending on the intention of the sequence programmer. It can also be a mere side effect of the flip back intention $\tilde{F}(0) \rightarrow \tilde{Z}(0)$. Please note that, without loss of generality for the results but for an improved visualization, a gradient along the y-axis instead of the z-axis was chosen for the linear harmonic wave patterns of the $\tilde{Z}$ states. [Color figure can be viewed in the online issue, which is available at wileyonlinelibrary.com.]

magnetization in the z-direction": The term derives from the fact that if non-coherent (i.e., $k \neq 0$) transverse magnetization components $\tilde{F}_+(k)$ and $\tilde{F}_-(-k)$ are converted into longitudinal $\tilde{Z}(k)$ states, they do not experience any phase evolution or dephasing anymore, i.e., their k remains constant. Modulated $\tilde{Z}$ states denote position encoded dephasing patterns and are "frozen". Additionally, being longitudinal magnetization, $\tilde{Z}$ states experience T_1 relaxation, which is usually much slower than T_2 relaxation (27,31).

As was already noted before, modulated z-magnetization can store a phase in terms of a shift of its modulation pattern in space (Fig. 7, c.f. chapter "Motion Phenomena"). The author still remembers an educational talk about phase graphs where the speaker claimed that the phase memory in the z-

direction cannot be explained; it would be a kind of "magic" or "mystery." On the contrary, it can be explained very well, as the present EPG concept demonstrates (10–17,23,27); it is just a phenomenon of the whole isochromat ensemble — it cannot be understood with one single isochromat only.

After discussing the importance of the triple of dephased and modulated magnetizations $\tilde{F}_+$, $\tilde{F}_-$, and $\tilde{Z}$, the focus is now on the coherent, not modulated configuration states with $k = 0$ (Fig. 7). The longitudinal $\tilde{Z}(0)$-state directly signifies equilibrium magnetization (11,13–15,18,27). It will be of particular importance in the section "Relaxation Effects." Exciting this magnetization with an RF pulse means to transfer population from $\tilde{Z}(0)$ to the coherent transverse magnetization component $\tilde{F}(0)$. Therefore, $\tilde{F}(0)$ states represent "freshly excited", coherent transverse magnetization, i.e., a free induction decay (FID) (Figs. 5 and 7). Maybe of even greater importance, $\tilde{F}(0)$ states also represent *echoes*. Thus, if during the evolution of an NMR sequence an $\tilde{F}(0)$-state occurs (not directly after excitation; see above), this coherent transverse magnetization corresponds to an echo. And quantifying the population of such an $\tilde{F}(0)$-state immediately means knowing the echo's intensity (the magnitude) and phase (the phase of the complex-valued population) (10–18). Thus, a very important assumption within the EPG framework is that all $\tilde{F}_+$ and $\tilde{F}_-$ states with $k \neq 0$ are fully dephased and, hence, do not contribute any signal to echo formation (c.f. chapter "Extensions, Limitations and Software Coding"). As longitudinal magnetization, $\tilde{Z}$ states will not contribute anyway.

Although they are two coherent transverse states $\tilde{F}_+(0)$ and $\tilde{F}_-(0)$, only the $\tilde{F}(0)$-state has been referred to, so far. The reason is that both states represent exactly the same information, however, they are complex conjugated to each other. So in the domain of the EPG concept, both states are equivalent but it is $\tilde{F}_-(0) = \left(\tilde{F}_+(0) \right)^*$. This can be seen from Eqs. (13a) and (13b) by defining $k = 0$. This small distinction is important to note, because it is one of the major reasons why people fail to use or program the EPG concept successfully, based on the experience of the author (c.f. chapter "Extensions, Limitations and Software Coding").

To make a short but important summary based on Eqs. (13a) to (13c) and (15) as well as Figure 7, the EPG concept explains that an SE will result from the phase reversal $\tilde{F}_+(k) \rightarrow \tilde{F}_-(-k)$, and that an STE will result from the excitation or stimulation of $\tilde{Z}(k) \rightarrow \tilde{F}_-(-k)$. In both cases $k \neq 0$. Frequently, measured echoes are a superposition of echoes of different configuration states (10–17,23–28).

Based on the general $\mathbf{T}$ operator in Eq. (15), the phase of spin and stimulated echoes can also be determined quite quickly. If ψ is the phase of the initial magnetization or state, and Φ_1 and Φ_2 are the phases of RF pulse 1 and 2, respectively, then (11)

$$\psi_{SE} = -\psi + 2\Phi_1 \text{ and} \qquad [16a]$$

$$\psi_{STE} = -\psi + \Phi_1 + \Phi_2. \qquad [16b]$$

Equations (13a) to (13c) represent the general continuous form of the EPG concept. Particularly for regular

and periodic MR sequences with equidistant timing, such as variants of TSE (4), SSFP (13,15,32–34) and Burst (35–37), only a discrete set of k-values is generated, if highly idealized conditions are presumed (c.f. chapter "Extensions, Limitations and Software Coding"). In this case, instead of using the spatial coordinate $\mathbf{r}$, it is more practical to use a dephasing angle $\theta = \theta(\mathbf{r})$ for Fourier decomposition (24):

$$M_+(\theta) = M_x(\theta) + iM_y(\theta) = \sum_{k=-\infty}^{\infty} \tilde{F}_k \cdot e^{ik\theta} \qquad [17a]$$

$$M_-(\theta) = M_x(\theta) - iM_y(\theta) = \left(\sum_{k=-\infty}^{\infty} \tilde{F}_k \cdot e^{ik\theta}\right)^*$$
$$= \sum_{k=-\infty}^{\infty} \tilde{F}_{-k}^* \cdot e^{ik\theta} \qquad [17b]$$

$$M_z(\theta) = \sum_{k=-\infty}^{\infty} \tilde{Z}_k \cdot e^{ik\theta} = Real\left(\sum_{k=0}^{\infty} \tilde{Z}_k \cdot e^{ik\theta}\right). \qquad [17c]$$

Several publications only present Eq. (17a) for the transverse magnetization approach, but either use both Eqs. (17a) and (17b) or make direct use of the complex conjugation property and the symmetry relations from Eqs. (14a) and (14b) (13–17,19,24,28). The latter approach, basically, combines Eq. (17a) for $k \geq 0$ and the right side of Eq. (17b) for $k < 0$. Because there are often no explicit comments on that, it is good advice to be aware of the full basis represented by Eqs. (17a) to (17c) and of the fact that there are symmetry relations. In the end, it is a matter of choice as to with which parts of the Fourier series one works (c.f. chapter "Extensions, Limitations and Software Coding").

Formulating [Eq. (15)] for the discrete k basis again, it is

$$\begin{bmatrix} \tilde{F}_k \\ \tilde{F}_{-k}^* \\ \tilde{Z}_k \end{bmatrix}^+ = \begin{bmatrix} \cos^2\frac{\alpha}{2} & e^{2i\Phi}\sin^2\frac{\alpha}{2} & -ie^{i\Phi}\sin\alpha \\ e^{-2i\Phi}\sin^2\frac{\alpha}{2} & \cos^2\frac{\alpha}{2} & ie^{-i\Phi}\sin\alpha \\ -\frac{i}{2}e^{-i\Phi}\sin\alpha & \frac{i}{2}e^{i\Phi}\sin\alpha & \cos\alpha \end{bmatrix}$$
$$\cdot \begin{bmatrix} \tilde{F}_k \\ \tilde{F}_{-k}^* \\ \tilde{Z}_k \end{bmatrix}^-. \qquad [18]$$

In the definition of Eqs. (17a) to (17c) and (18), k represents an integral number describing the state's dephasing in units of 2π (over a voxel or a volume). This approach is really useful in practice, because the index k also depicts how many intervals of TR (for SSFP sequences), RFSP (for Burst sequences) or ESP/2 (for TSE sequences), magnetization is dephased ($\tilde{F}_k$ states), magnetization will become coherent to generate an echo if left unaffected ($\tilde{F}_{-k}^*$ states), or magnetization was dephasing or rephasing before it got longitudinal ($\tilde{Z}_k$ states) (10–17,23,24,28).

Figure 8 illustrates the direct graphical meaning of the discrete, integral configuration states. Equation (18) depicts the exchange of populations due to RF pulses between the configuration states of the same $|k|$ (which are in the same column in Fig. 8). It also clarifies what sequence experts ("insiders") exactly mean when they discuss $\tilde{F}_{-1}$ states, stimulated ech-

oes deriving from $\tilde{Z}_3$ states, etc. It should be noted that all $\tilde{F}_{-k}$ states, i.e., $k < 0$, usually refer to the rephasing configurations in the literature, even if it does not explicitly say $\tilde{F}_{-k}^*$ (typical discrete notation) or $\tilde{F}_-(-k)$ (concise general notation).

In this work, the author refrains from applying different notations for dimensionless, integral k and for real k according to Eq. (4) in the unit rad/m. As long as the k values are not used for calculating populations of configuration states directly, the integral ones can be used (c.f. section "Motion Phenomena").

Short Examples in Regard to the *T*-Operator

To deepen the feeling for the partitioning effect of the $\mathbf{T}$-matrix operator, the two special cases $\mathbf{T}_x(180°)$ and $\mathbf{T}_x(90°)$ are investigated. Without loss of generality for the partitioning effect, the magnetization is rotated around the x-axis:

$$\mathbf{T}_x(180°) = \begin{bmatrix} 0 & 1 & 0 \\ 1 & 0 & 0 \\ 0 & 0 & -1 \end{bmatrix} \text{ and } \mathbf{T}_x(90°) = \begin{bmatrix} \frac{1}{2} & \frac{1}{2} & -i \\ \frac{1}{2} & \frac{1}{2} & +i \\ -\frac{i}{2} & \frac{i}{2} & 0 \end{bmatrix}. \qquad [19]$$

The *T*-matrices in Eq. (19) demonstrate that a $180°$ RF pulse swaps the populations of the $\tilde{F}$ states (perfect refocusing, full defocusing) and negates the sign of the $\tilde{Z}$ states (inversion). By contrast, a $90°$ RF pulse keeps half of the population in each of both $\tilde{F}$ states and swaps the other half between them (half refocusing and defocusing). It converts all $\tilde{Z}$ into $\tilde{F}$ magnetization (excitation, stimulated echo) and also converts half of the transverse into longitudinal magnetization (storage, flip back). The latter is the reason that the basic stimulated echo sequence $90°$-$90°$-90, already described by Hahn, has the relative signal intensity of $1/2$ only (1,38).

Real Valued Representations Within the EPG

In the EPG concept, transverse magnetization is depicted as complex $\tilde{F}_+$ and $\tilde{F}_-$ due to its 2D properties. If all RF pulses used have the same RF phase, i.e., identical precession axes, and if the initial magnetization/the initial EPG states are either parallel or orthogonal in phase to all RF pulses, all successive spin and stimulated echoes are generated on the same axis in the x-y-plane (c.f. Eqs. (16a) and (16b)). The first case is called *in-phase refocusing* and takes place in the popular CPMG sequence (1–3); the second case is called *out-of-phase refocusing* and takes place in the Carr-Purcell (CP) sequence (1,2) and in particular types of SSFP without RF spoiling (12,13,15).

It should be noted that for the case of out-of-phase refocusing the SE and the STE are in antiphase with respect to each other, thus, one also refers to the anti-CPMG component. This term will be used from now on.

In both cases, the coordinate system can be rotated and redefined such that magnetization always refocuses on the real-valued x-axis. As a result, a purely
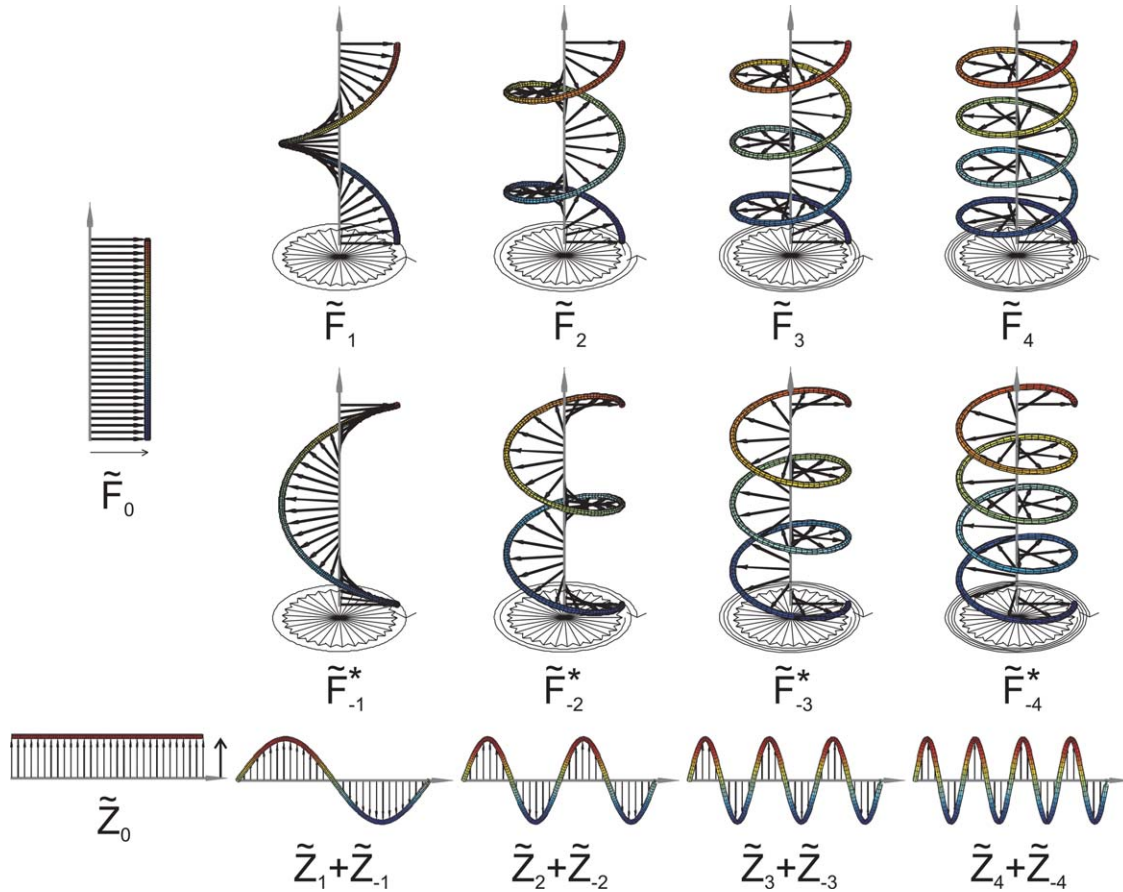
Figure 8. Graphical representation of the first four discrete configuration states with integral k. Each state has a dephasing of $2\pi k$. In the first row with $k > 0$ are the dephasing configurations, in the second row with $k < 0$ the corresponding counter-rotated helices, the rephasing configurations. Both share one coherent F_0 state which is redundant by conjugation. All transverse states are perfectly dephased except for the F_0 state. The helix projections may be recognized from different previous publications by Hennig and Scheffler (11,15). The third row displays in each case the combination of both longitudinal configuration pairs, being together a linear, harmonic wave pattern. Again, without loss of generality but for an improved visualization, a gradient along the y-axis instead of the z-axis was chosen for the linear harmonic wave patterns of the Z states. [Color figure can be viewed in the online issue, which is available at wileyonlinelibrary.com.]

real representation for $\tilde{F}_{\pm}(k)$ and $\tilde{Z}(k)$ configuration states exists. This purely real representation has the advantage that one does not have to worry about complex conjugate operations anymore (c.f. chapter "Extensions, Limitations and Software Coding"). $\tilde{F}_+(k)$ and $\tilde{F}_-(k)$ become identical and degenerate to a $\tilde{F}(k)$. Hence, the population exchange takes place easily between $\tilde{F}(+k)$, $\tilde{F}(-k)$, and $\tilde{Z}(k)$. Depending on the software implementation of the computer, the EPG concept may also become more simple to program. The only change necessary to achieve a real representation is to find the appropriate real-valued **T** operator; as a consequence, all configuration states will be real.

To derive the anti-CPMG-representation, a thought experiment can be performed: Starting with (real) equilibrium magnetization using a $\mathbf{T}_{90°}(\alpha)$ operator, i.e., defining $\Phi = 90°$ in Eq. (15), it can be shown that only EPG states $\tilde{F}_{\pm}(k)$ and $\tilde{Z}(k)$ with pure real populations are generated in succession. Thus, all imaginary parts vanish permanently and the description is consistent. Therefore, the resulting **T** operator to use is

$$\mathbf{T}_{\text{anti-CPMG}}(\alpha) = \begin{bmatrix} \cos^2\dfrac{\alpha}{2} & -\sin^2\dfrac{\alpha}{2} & \sin\alpha \\[2mm] -\sin^2\dfrac{\alpha}{2} & \cos^2\dfrac{\alpha}{2} & \sin\alpha \\[2mm] -\dfrac{1}{2}\sin\alpha & -\dfrac{1}{2}\sin\alpha & \cos\alpha \end{bmatrix}. \quad [20]$$

Besides CP-based spin echo sequences, the $\mathbf{T}_{\text{anti-CPMG}}$ (α) operator could be also used to simulate balanced SSFP with and without alternating phase (TrueFISP) and further steady state sequences without RF spoiling like FISP (12,13,15).

For deriving the CPMG representation, a similar though experiment can be performed: As an initial condition, magnetization is solely present as transverse magnetization on the real x-axis. The longitudinal components are redefined by means of $\tilde{Z}(k) \rightarrow i \cdot \tilde{Z}(k)$. Then, using a $\mathbf{T}_{0°}(\alpha)$ operator, i.e., defining $\Phi = 0°$ in Eq. (15), it can be shown that only EPG states $\tilde{F}_{\pm}(k)$ and $\tilde{Z}(k)$ with pure real populations are generated permanently in succession and that the description is consistent. Therefore, the resulting **T** operator to use is

$$\mathbf{T}_{\mathrm{CPMG}}(\alpha) = \begin{bmatrix} \cos^2\dfrac{\alpha}{2} & \sin^2\dfrac{\alpha}{2} & \sin\alpha \\[2mm] \sin^2\dfrac{\alpha}{2} & \cos^2\dfrac{\alpha}{2} & -\sin\alpha \\[2mm] -\dfrac{1}{2}\sin\alpha & \dfrac{1}{2}\sin\alpha & \cos\alpha \end{bmatrix}. \qquad [21]$$

The CPMG scheme is the basis for the popular TSE sequence and its derivatives (4). Thus, the $\mathbf{T}_{\mathrm{CPMG}}(\alpha)$ operator is used regularly for EPG based simulations of TSE-like sequences (10–12,23,27,29,31,35,38–42).

Please note that the signs of the $\mathbf{T}_{\mathrm{CPMG}}(\alpha)$ operator are not entirely correct in Ref. (23). Additionally, there is a contradiction between the 4-state EPG $\mathbf{T}_{\mathrm{CPMG}}(\alpha)$ operators used in Refs. (10–12) (c.f. chapter "Graphical Representation").

Dephasing Due to Gradients

Because the EPG concept is built on Fourier based dephasing states, dephasing effects caused by gradients are implemented by means of the shift operator **S** in a simple way (10–17,19,23–29):

$$\mathbf{S}(\Delta k): \qquad \tilde{F}_k \to \tilde{F}_{k+\Delta k} \ \text{ and } \ \tilde{Z}_k \to \tilde{Z}_k \qquad [22]$$

if the gradient has the 0th moment of $\Delta k = \gamma \int_{t'=0}^{t} G(t')\, dt'$. This relation can be proven by inserting the Fourier decompositions of Eqs. (13) or (17) into the $\mathbf{T_z}$-matrix in Eq. (11), as demonstrated in Refs. (16,24).

Equation (22) confirms the well-known effect that only transverse $\tilde{F}_\pm(k)$ states experience phase evolution, whereas longitudinal $\tilde{Z}(k)$ states do not.

If periodic sequences are investigated, Δk can be merely an integral number, usually 1 or 2 depending on the timing character of the sequence (see Eqs. (17) and (18) with text above). Please note that this simplification is only valid, if the EPG operators used do not depend on the absolute value of k. Otherwise further considerations have to be taken into account (c.f. section "Motion Phenomena") (18).

Relaxation Effects

The EPG concept maintains the "natural anisotropy" between longitudinal and transverse magnetization in regard to dephasing, relaxation or diffusion effects. Thus, relaxation phenomena are included simply by the operator (10–12,15,17–19,23,27,29–31)

$$\mathbf{E}(\tau, T_1, T_2) = \begin{bmatrix} E_2 & 0 & 0 \\ 0 & E_2 & 0 \\ 0 & 0 & E_1 \end{bmatrix} \qquad [23]$$

for $k \neq 0$ states.

The common abbreviations $E_1 = \exp(-\tau/T_1)$ and $E_2 = \exp(-\tau/T_2)$ were used (15), with T_1 and T_2 being the relaxation times and τ the time interval given. Please note that relaxation operator **E** is a fully signal destructive operator: All configuration states with $k \neq 0$, i.e., also longitudinal states, decay inevitably due to T_1 or T_2 relaxation, because these are off equilibrium.

For $k = 0$, additional T_1 recovery toward thermal equilibrium magnetization $M_0 = 1$ has to be considered for $\tilde{Z}(0)$. Hence, Eq. (23) changes to the relation

$$\begin{bmatrix} F_+ \\ F_- \\ Z \end{bmatrix}^+ = \begin{bmatrix} E_2 & 0 & 0 \\ 0 & E_2 & 0 \\ 0 & 0 & E_1 \end{bmatrix} \cdot \begin{bmatrix} F_+ \\ F_- \\ Z \end{bmatrix}^- + \begin{bmatrix} 0 \\ 0 \\ M_0\,(1 - E_1) \end{bmatrix}$$
$$[24]$$

for $k = 0$ states,

where the full matrix-vector relation is written out such that an addition of the recovering magnetization is possible (last term on the right side) (15,18,23).

Finalizing the Fundamental Extended Phase Graph Framework

In practice, the complete ensemble magnetization is described as the sum of different configuration states at any time during the NMR sequence (10–19,25,25,28,28,43). This set of defining configuration states is usually stored in a state vector (11,18)

$$\mathbf{F} = \left[\tilde{F}_{k_0}, \tilde{F}_{k_1}, \tilde{F}_{k_2}, \ldots, \tilde{F}_{-k_3}, \tilde{F}_{-k_4}, \tilde{F}_{-k_5}, \ldots, Z_{k_6}, Z_{k_7}, Z_{k_8}\ldots\right]^{\mathrm{T}}$$
$$[25]$$

or, particularly for regular EPGs, in a state matrix (18,19)

$$\mathbf{\Omega} = \begin{bmatrix} \tilde{F}_0 & \tilde{F}_1 & \tilde{F}_2 & \tilde{F}_3 & \tilde{F}_4 & \tilde{F}_5 & \cdots \\ \tilde{F}_0^* & \tilde{F}_{-1}^* & \tilde{F}_{-2}^* & \tilde{F}_{-3}^* & \tilde{F}_{-4}^* & \tilde{F}_{-5}^* & \cdots \\ \tilde{Z}_0 & \tilde{Z}_1 & \tilde{Z}_2 & \tilde{Z}_3 & \tilde{Z}_4 & \tilde{Z}_5 & \cdots \end{bmatrix} \qquad [26]$$

where $\mathbf{\Omega}$ corresponds to a sequencing of the three base states along an increasing dephasing order k. Please note that in this representation $\tilde{F}_0$ occurs twice in the two modifications $\tilde{F}_+$ and $\tilde{F}_-$, so care is advised (c.f. chapter "Extensions, Limitations and Software Coding"). Whereas the latter state matrix (Eq. (26)) gives a better overview and already resembles the way a programmer would probably store and handle the data in a computer program for regular EPGs, the former column vector **F** (Eq. (25)) is more practical to build the two state evolution matrices

$$\Xi_F = \begin{pmatrix} \vdots & \vdots & \vdots & \vdots & \vdots \\ \tilde{F}_2(t_0) & \tilde{F}_2(t_1) & \tilde{F}_2(t_2) & \tilde{F}_2(t_3) & \cdots \\ \tilde{F}_1(t_0) & \tilde{F}_1(t_1) & \tilde{F}_1(t_2) & \tilde{F}_1(t_3) & \cdots \\ \tilde{F}_0(t_0) & \tilde{F}_0(t_1) & \tilde{F}_0(t_2) & \tilde{F}_0(t_3) & \cdots \\ \tilde{F}_{-1}^*(t_0) & \tilde{F}_{-1}^*(t_1) & \tilde{F}_{-1}^*(t_2) & \tilde{F}_{-1}^*(t_3) & \cdots \\ \tilde{F}_{-2}^*(t_0) & \tilde{F}_{-2}^*(t_1) & \tilde{F}_{-2}^*(t_2) & \tilde{F}_{-2}^*(t_3) & \cdots \\ \vdots & \vdots & \vdots & \vdots & \ddots \end{pmatrix}$$
$$[27a]$$

and

$$\Xi_Z = \begin{pmatrix} \vdots & \vdots & \vdots & \vdots & \vdots \\ \tilde{Z}_2(t_0) & \tilde{Z}_2(t_1) & \tilde{Z}_2(t_2) & \tilde{Z}_2(t_3) & \cdots \\ \tilde{Z}_1(t_0) & \tilde{Z}_1(t_1) & \tilde{Z}_1(t_2) & \tilde{Z}_1(t_3) & \cdots \\ \tilde{Z}_0(t_0) & \tilde{Z}_0(t_1) & \tilde{Z}_0(t_2) & \tilde{Z}_0(t_3) & \cdots \\ \tilde{Z}_1^*(t_0) & \tilde{Z}_1^*(t_1) & \tilde{Z}_1^*(t_2) & \tilde{Z}_1^*(t_3) & \cdots \\ \tilde{Z}_2^*(t_0) & \tilde{Z}_2^*(t_1) & \tilde{Z}_2^*(t_2) & \tilde{Z}_2^*(t_3) & \cdots \\ \vdots & \vdots & \vdots & \vdots & \ddots \end{pmatrix}, \quad [27b]$$

which depict the evolution of an NMR sequence within the EPG concept at discrete points of time. For reasons of consistency with regard to the Ξ_F state evolution matrix, Ξ_Z also includes the complex conjugated "partner" $\tilde{Z}_{-k}^*$. The evolution of a given NMR sequence is depicted by the different physical operators that modify $\mathbf{F}$ or Ω to account for effects such as dephasing, relaxation, and diffusion (18,19):

$$\mathbf{F}(t) = \; \dots \; \mathbf{E\,S\,J\,D\,T\,E\,S\,J\,D\,T}\;\mathbf{F}(t=0) \qquad [28a]$$

$$\Omega(t) = \; \dots \; \mathbf{E\,S\,J\,D\,T\,E\,S\,J\,D\,T}\;\Omega(t=0). \qquad [28b]$$

Hence, $\mathbf{F}(t)$ or $\Omega(t)$ is calculated by means of successive operator matrix applications acting on an initial $\tilde{F}_0$ or $\tilde{Z}_0$ state, for instance. The operators $\mathbf{E}$, $\mathbf{J}$, and $\mathbf{D}$ used in Eqs. (28a) and (28b), representing relaxation, flow and diffusion, will be introduced later. Generally, the operators do not commute; thus, one has to define carefully in which order they are to be used.

Generally, with time the state vector and state matrix will increase in size so as to include states of higher order k that are generated. However, exactly speaking from a physical point of view, it is not that new configuration states are generated or come into existence; it is more correct to say (and think) of the EPG evolution that it occupies states of higher order k with a non-zero population (18). The configuration states are already there. In fact, the state vector and state matrix have infinite size and contain all states that the sequence can access; however, they initially have a zero population (18). So these states are just omitted for reasons of simplicity and brevity (18).

If magnetization decay effects such as relaxation or diffusion are omitted, the macroscopic net magnetization is preserved and, thus, the sum of the square of the absolute value of each configuration state stays constant and is equal to the equilibrium magnetization $M_0 = 1$ (11,23):

$$\sum_{k=-\infty}^{\infty} |F_k|^2 + |Z_k|^2 = |F_0|^2 + |Z_0|^2 + \sum_{k=1}^{\infty} |F_k|^2 + |F_{-k}|^2$$
$$+ 2 \cdot |Z_k|^2$$
$$= 1.$$
$$[29]$$

The mathematical operation $||^2$ signifies the square of the absolute value and is defined as $|\rho|^2 = \rho \cdot \rho^*$ for a complex population ρ. The reader should note that Hennig's original formulations (11,23) are only valid for real EPGs based on the $\mathbf{T}_{CPMG}(\alpha)$ operator from Eq. (21).

At this point, the foundation of the EPG concept is complete: Magnetization is depicted by means of Fou-

rier based configuration states, gradients modify the dephasing order of these, and RF pulses exchange populations between these configuration states of identical order k. As a result, Figure 9 presents how these achievements can be used to solve the original questions put forth in reference to Figure 1.

As a *historical side note*, the word "extended" in the acronym EPG refers to Hennig's reinterpretation of the partition state (original phase graph) method by means of Fourier based configuration states (7–12). Although termed "extended" by Hennig some 20 years ago, it is rather a significant discrimination than a mere extension. Often users are not aware of this significant difference, because the graphical and mathematical representation of both phase graph interpretations looks very similar.

While the focus of Woessner and Kaiser et al with the partition state and Fourier expansion method was on the understanding of diffusion weighting in multi-echo sequences (8,9), the focus of Hennig was on the understanding of echo generation in imaging sequences (10–12). Actually, MRI had just arrived on the scene (44–46) when Kaiser published the partition state method (8,9).

Graphical Representation: Extended Phase Diagrams

Besides the analytical and numerical foundation of the EPG concept, there is significant attention being focused on actually drawing the evolution of the configuration states in *extended phase diagrams*. A set of configuration states characterize the isochromat ensemble at a given time, but (magnetization) pathways connect these configuration states to illustrate how these states evolve during the action of RF pulses as well as of dephasing due to gradients, etc., over time. The literature does frequently use the terms "state" and "pathway" interchangeably; yet, the focus lies on different aspects.

For, so to speak, reading (or tracing) the magnetization response, the configuration states are located on the y-axis and time on the x-axis (Fig. 10). The actual populations are not shown in this diagram; here of more interest are the possible configurations the system can occupy as a function of time. Presenting all available information of the Fourier based EPG concept $\tilde{F}_+(\pm k)$, $\tilde{F}_-(\pm k)$, and $\tilde{Z}(\pm k)$ in a graphical diagram leads merely to confusion than precise results (Fig. 10a). However, based on the symmetry relations in Eqs. (14a) and (14b) redundant information can be omitted. This redundancy is solved best for the diagrams by omitting all configuration states that depend on $-k$, because a given gradient should always act consistently on transverse magnetization over the whole range of dephasing displayed on the y-axis. Hence, at times when a solid line, representing transverse magnetization, intersects the x-axis, coherent magnetization exists, which corresponds to echo generation ($\tilde{F}(0)$ state, Fig. 10b). The $\tilde{Z}(-k)$ states do not add new information to the diagram. This results in the extended phase diagram representation $\tilde{F}_+(k)$, $\tilde{F}_-(k)$, and $\tilde{Z}(k)$ in Figure 10b as it is common today.
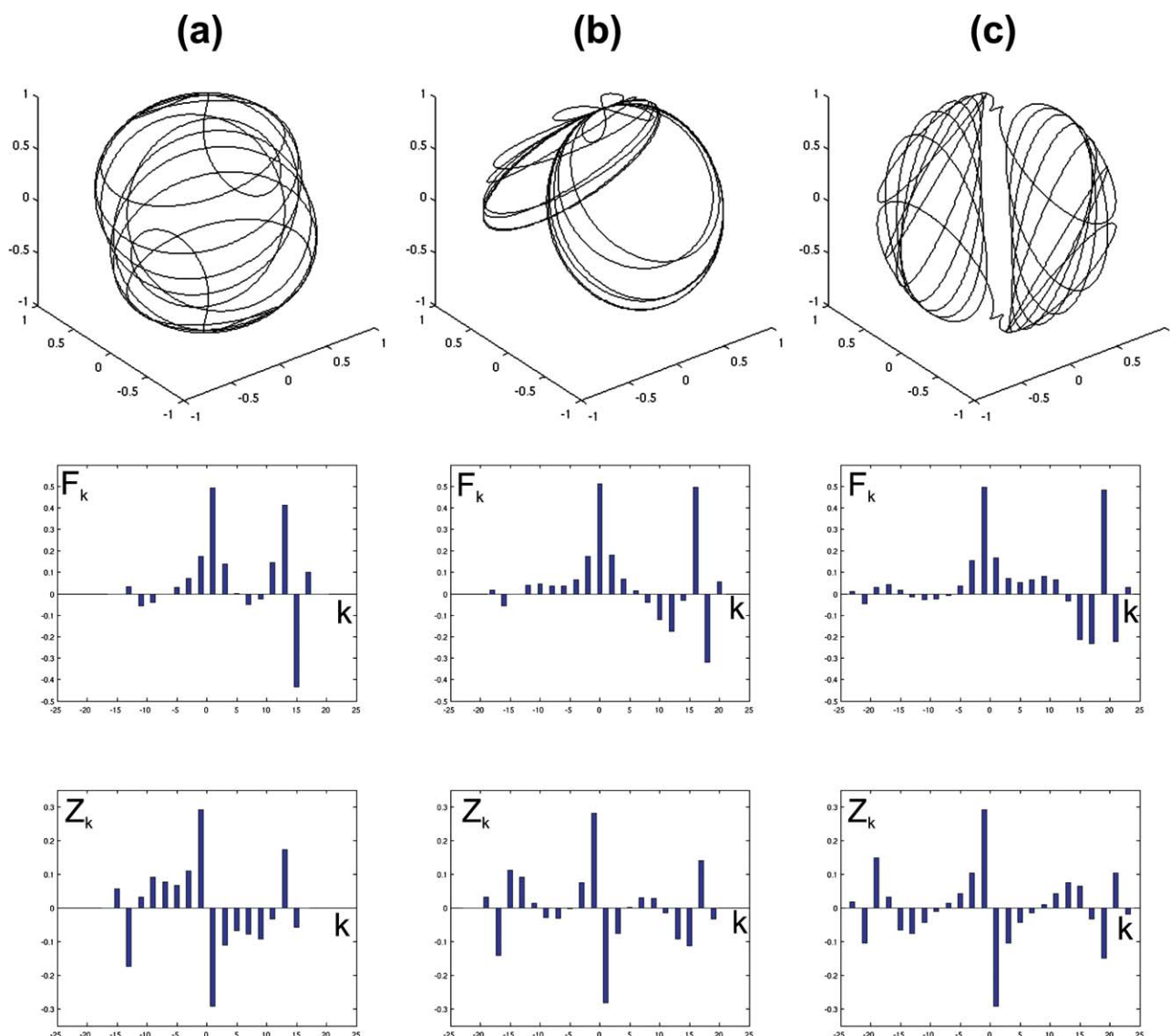
(a) (b) (c)

Figure 9. Taking up the example of Figure 1, the presented isochromat ensemble configurations can be quantified simply and precisely by the populations of configurations states, as shown by the histograms. Because time increases from (a) to (c), states of higher order k are occupied. Now, a quick glance reveals that the F_0 state is not occupied in constellations (a) and (c); thus, these are completely dephased systems. So the constellations cannot represent a (partial) echo. The F_0 state in constellation (b), however, is occupied with 0.5, the echo intensity! Because the simulation was performed without relaxation effects, no T_1 recovery is present, which leads to even Z states and every other F state being 0 (CPMG timing, see examples later). The Z states display the inherent symmetry based on the symmetry relations. Note that these simulations were performed with the real operator $\mathbf{T}_{\mathrm{CPMG}}$ in Eq. (21). With the previous knowledge of $T_1 = T_2 = \infty$ and $\alpha_{\mathrm{const}} = 60°$, even the interval of the sequence can be guessed by the maximal $|k|$ occurring. [Color figure can be viewed in the online issue, which is available at wileyonlinelibrary.com.]

As a side note, this diagram is very similar to the presentation one gets with the partition state method.

It should be noted that EPG diagrams often ignore the intricacies of $k(t)$ trajectories, i.e., they do not necessarily reflect the real trajectory. EPGs represent "dephasing" in a very general sense; thus, its source may be chemical shift, B_0 inhomogeneities, J-coupling, etc., besides the very frequent read gradient as a 1D dephasing axis (11). Hence, k should generally not be on the y-axis either. Regularly, the real gradient waveforms are ignored and replaced with a constant time-filling gradient of the same moment, thus leading to linear pathways in the diagram.

Sodickson and Cory tagged EPGs as a "generalized k-space formalism" (14). Considering the facts discussed above, this does not seem to be really helpful, but rather leads to confusion. Besides, k-space has a different focus and is mostly concerned with imaging behavior rather than with echo generation. k-space ignores longitudinal magnetization and includes $180°$ pulses at most. However, if motion phenomena are to be included, correct calculations with exact $k(t)$ trajectories become important (c.f. chapter "Motion Phenomena").

Generally, the splitting of RF pulses leads to an exponential increase of pathways with the number of
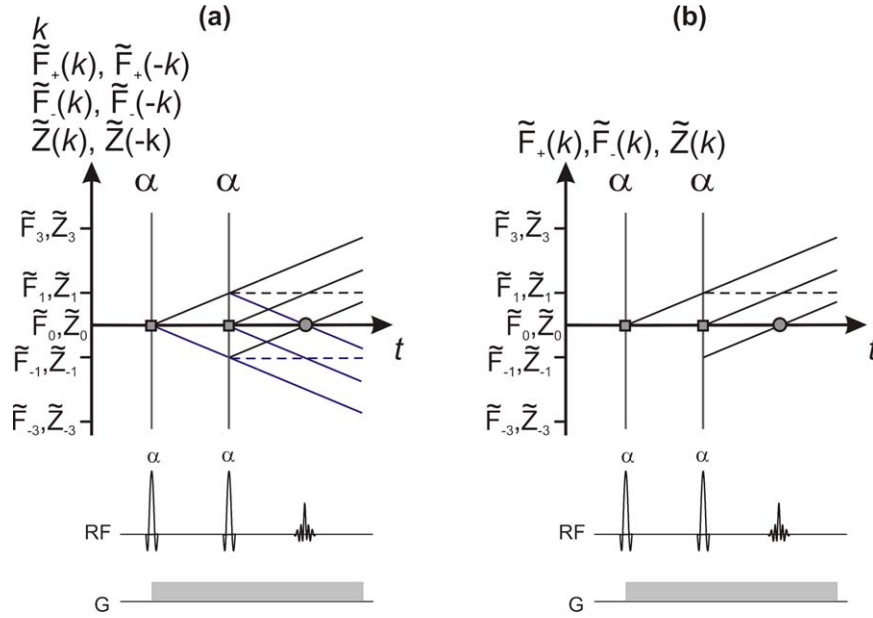
Figure 10. Extended phase diagram of a two-pulse sequence that may be the beginning of a Burst sequence (35–37). $\tilde{F}$ state pathways are represented by solid lines and their slope is proportional to the gradient strength. $\tilde{Z}$ state pathways are signified by dashed lines. These are always horizontal, because they show no phase evolution. RF pulses are signified by a vertical line. They split each existing pathway and generate a new FID from residual and "freshly recovered" longitudinal magnetization (square markers). **a:** Showing all Fourier components of the EPG leads to a rather useless diagram. Considering that a gradient should always act on transverse magnetization in the same sense and one is used to increasing dephasing, i.e., increasing k, in the positive direction of the y-axis, results in the exclusion of the two redundant $\tilde{F}$ components depending on $-k$. Thus, dephasing transverse magnetization corresponds to the diagonal solid line above $\tilde{F}(0)$, i.e., the x-axis, and rephasing to those below the line $\tilde{F}(0)$. Therefore intersections with the x-axis denote the generation of an echo (disc marker, $\tilde{F}(0)$ state). This procedure leads to the four-state diagram ($\tilde{F}_+(+k)$, $\tilde{F}_-(+k)$, $\tilde{Z}(+k)$, $\tilde{Z}(-k)$) originally used by Hennig (10–12). However, $\tilde{Z}(-k)$ is also redundant; hence, it is taken out. **b:** The resulting diagram style common today ($\tilde{F}_+(k)$, $\tilde{F}_-(k)$, $\tilde{Z}(k)$). It may be a matter of discussion whether the spatial frequency k itself should be or even is allowed to be on the y-axis. Indeed, this direction represents dephasing, however, in a rather generalized sense (c.f. text). Thus, according to the view of the author, "k" should only be present if the extended phase diagram directly reflects the true $k(t)$ trajectory. Corresponding examples are Figure 18 in this work and Figure 1 in Ref. (18). [Color figure can be viewed in the online issue, which is available at wileyonlinelibrary.com.]

RF pulses N. Starting from one initial pathway, an RF pulse splits all pathways into three new parts and generates one new FID. Each successive RF pulse will split up each pathway again, including the former FID; and it will generate an FID of its own. Accordingly, the geometric series

$$n_{\text{pathways}}(N) = 3^N + 3^{N-1} + \ldots + 3^1 + 3^0 = \sum_{l=0}^{N} 3^l$$
$$= \frac{1}{2} \left(3^{N+1} - 1\right) \xrightarrow{N \to N-1} \frac{1}{2} \left(3^N - 1\right)$$

[30]

depicts the number of pathways n generated altogether, if the first pulse is treated as the excitation pulse generating the initial pathway. Please note that the equilibrium configuration state $\tilde{Z}_0$ is not regarded as a pathway.

Classification of Echoes

One of the original questions put forth was whether a general classification of echoes can be introduced. For this task, a generic SE sequence with three nonequidistant RF pulses with arbitrary flip angles α_1, α_2, and α_3 is investigated in Figure 11. The RF pulse phases do not matter, because they influence the echo phases only (see above).

The EPG in Figure 11 beautifully demonstrates how the RF pulses split the pathways. In dependence on the magnetization history before the last RF pulse, an SE or an STE is present. It is suggested to further characterize the echoes by means of indexing here: The number of each RF pulse actively participating in the echo generation is noted as a successive subscript index, starting with the FID generating RF pulse. An FID directly acquires its corresponding RF pulse number. Thus, reading from either Figure 11 or the indexing method, it is immediately clear that at least three RF pulses are necessary to generate an STE, which becomes $STE_{1\text{-}2\text{-}3}$: (i) FID_1, (ii) storing as a modulated Z-state, (iii) stimulation to generate the $STE_{1\text{-}2\text{-}3}$.

Using the indexing method for spin echoes results in $SE_{1\text{-}2\text{-}3}$, $SE_{1\text{-}3}$, $SE_{1\text{-}2}$ and $SE_{2\text{-}3}$. Depending on whether the echoes trace back to FID_1 (first echo index is 1) or a later FID (first echo index is greater than 1), the spin echo is sub-classified to be primary or secondary (Fig. 11). These terms originate from Hahn's paper (1). With the EPG based indexing method these can be characterized more precisely.

Examples for MRI Sequences

After the thorough discussion of its basis and properties, the established EPG framework will be put into

Figure 11. Extended phase graph for an arbitrary three-pulse spin echo sequence. Based on the EPG diagram, the identification and classification of echoes is intuitive and simple: The three RF pulses excite three new FIDs, generate one stimulated echo (STE) from a longitudinal pathway, and refocus four transverse pathways to spin echoes (SE). Applying the recommended indexing of echoes based on the RF pulses (see text) leads to the further sub-classification into three primary spin echoes (SE_{1-2}, SE_{1-2-3}, SE_{1-3}) and one secondary spin echo (SE_{2-3}). The corresponding echo times of generation are clear. In the end $\frac{1}{2}(3^3 - 1) = 13$ pathways are observed (Eq. (30)).
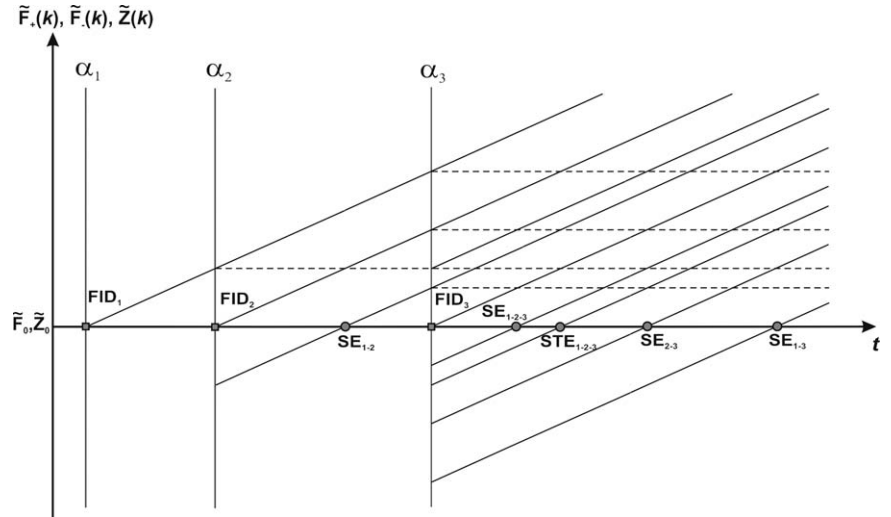
practice. However, an in-depth discussion of the sequences and many possibilities using the EPG concept is beyond the scope of this review. It is obvious that multi-pulse sequences such as (and not restricted to) variants of TSE, SSFP, and Burst as well as DANTE approaches highly benefit from the presented EPG framework. Thus, the reader is referred to the abundant dedicated literature such as Refs. (4,8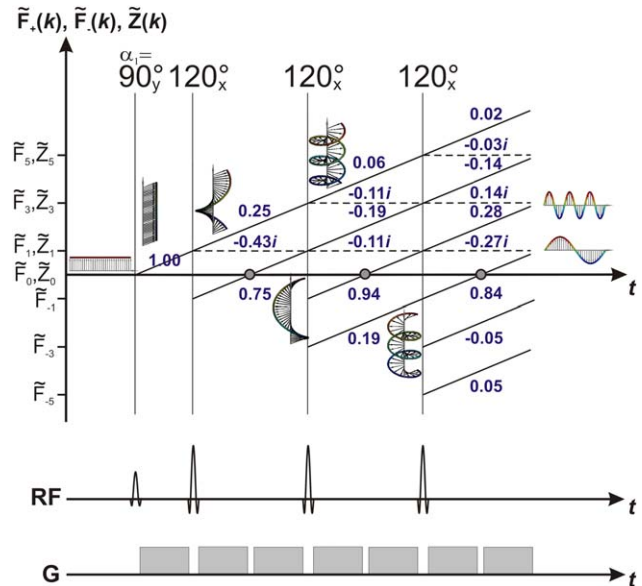–19,23,25–27,29,31–43,47–62). Apart from reading the best way to get more insight into and, most importantly, to get an intuitive feeling for the EPG framework is to try out ideas and draw examples, calculate around, and definitely think about it.

$$\mathbf{T_y}(90^\circ) = \begin{bmatrix} 0.50 & -0.50 & 1 \\ -0.50 & 0.50 & 1 \\ -0.50 & -0.50 & 0 \end{bmatrix}$$

and

Example: Simulating Turbo Spin Echo Sequences

The basic magnetization response of a TSE (CPMG) sequence with constant 120° refocusing flip angles and echo spacing ESP (4,10,11) is investigated neglecting relaxation effects (Fig. 12). The read encoding direction of the TSE sequence determines its basic magnetization response in regard to echo generation. It should be noted that EPGs are also feasible in other encoding directions such as the 2D phase or 3D partition encoding direction; Weigel and Hennig demonstrated this possibility by quantitating the inherent diffusion sensitivity of TSE sequences for the different encoding axes (58).

As can be easily seen in Figure 12, TSE sequences recombine EPG pathways of equal order due to the regular timing and coherence conditions of gradients and RF pulses: An only linear increase of pathways with the number N of RF pulses can be observed in Figure 12 (11,15,16,18). This result is true for all NMR sequences of regular or periodic timing.

In accordance with Figure 12, the magnetization evolution will be simulated based on the EPG framework using the state matrix of Eq. (26) and following Eq. (28b). At first, the appropriate **T** operators are defined. To obey the CPMG condition, the 90° excitation does have an RF phase of $\Phi = 90^\circ$ (y-axis), whereas all 120° refocusing pulses have $\Phi = 0^\circ$ (x-axis) (Eq. (15)):

Figure 12. Extended phase diagram of a TSE sequence including a simplified sequence diagram of its read encoding direction (crusher and read out gradients are one). The first RF pulse excites magnetization to become an FID (the primary echo pathway), which the successive RF pulses split. Only odd states are linked by the primary pathways at the times of the RF pulses (CPMG timing). The blue numbers denote the population of each pathway based on the example for constant 120° refocusing flip angles and no relaxation effects. With T_1 recovery present, each refocusing pulse would generate an FID that would lead to secondary SEs occurring at the time of the RF pulses. Thus, they cannot be observed in a TSE sequence. This strict separation of primary and secondary SE pathways leads to the inevitable decay of magnetization along the echo train. Imagine analyzing these behaviors without phase graphing!

$$\mathbf{T_x}(120^\circ) = \begin{bmatrix} 0.25 & 0.75 & -0.87i \\ 0.75 & 0.25 & 0.87i \\ -0.43i & 0.43i & -0.50 \end{bmatrix}. \qquad [31]$$

Starting with equilibrium magnetization (Fig. 12) the initial state matrix is $\mathbf{\Omega}(t < 0) = [0, 0, 1]^T$. At $t = 0$, the excitation pulse changes the state matrix to be

$$\mathbf{\Omega}(t = 0) = \mathbf{T_y}(90^\circ)\,\mathbf{\Omega}(t < 0) = \begin{bmatrix} F_0 \\ F_0^* \\ Z_0 \end{bmatrix} = \begin{bmatrix} 1 \\ 1 \\ 0 \end{bmatrix}. \qquad [32]$$

Again, it is emphasized that both $\tilde{F}_0$ are complex conjugated partners, they are the same state in this representation (c.f. chapter "Extensions, Limitations and Software Coding." The result of Eq. (32) corresponds to the expectation: The equilibrium magnetization is rotated to become positive x-magnetization completely. Next, the $\mathbf{S}$ operator acts and shifts all states up, i.e. the positive dephasing gradient in the first interval increases the k of all transverse states by 1 (Fig. 12). Thus, the state matrix has to be increased to make room for the newly populated $\tilde{F}_1$ state:

$$\mathbf{\Omega}\left(t = \frac{1}{2}ESP^-\right) = \mathbf{S}\,\mathbf{\Omega}(t = 0) = \begin{bmatrix} 0 & 1 \\ 0 & 0 \\ 0 & 0 \end{bmatrix}. \qquad [33]$$

In Eq. (33), the superscript "−" means "directly before", the later superscript "+" will mean directly after. Because there is no T1 recovery, the $\tilde{Z}_0$ population remains 0.

Now, the first refocusing pulse represented by the $\mathbf{T_x}(120^\circ)$ operator is applied (Fig. 12), mixing states of equal dephasing order k:

$$\mathbf{\Omega}\left(t = \frac{1}{2}ESP^+\right) = \mathbf{T_x}(120^\circ)\,\mathbf{\Omega}\left(t = \left(\frac{1}{2}ESP\right)^-\right)$$
$$= \begin{bmatrix} 0 & 0.25 \\ 0 & 0.75 \\ 0 & -0.43i \end{bmatrix}. \qquad [34]$$

The RF pulse partitions the former $\tilde{F}_1$ state into the fractions 0.25 of further dephasing magnetization, 0.75 of rephasing magnetization, and 0.43 of stored longitudinal magnetization. The additional factor $-i$ of $\tilde{Z}_1$ hints at the phase of the magnetization. Because no longitudinal magnetization is recovered, $\tilde{Z}_0 = 0$, the RF pulse could not excite magnetization generating an FID (c.f. Fig. 11): the $\tilde{F}_0$ state remained with the population 0. As a consequence, no secondary SEs will be generated at all (c.f. Fig. 11) and these pathways were omitted in Figure 12. Generally, refocusing pulses generate FIDs in a TSE sequence that result in secondary SEs; however, these occur during the time of the refocusing pulses and are, therefore, never observed. Thus, these secondary pathways are seldom found in extended phase diagrams from TSE sequences (27).

Next, the first half of the readout gradient follows, denoted by the same shift operator from above:

$$\mathbf{\Omega}(t = ESP) = \mathbf{S}\,\mathbf{\Omega}\left(t = \frac{1}{2}ESP^+\right)$$
$$= \begin{bmatrix} 0.75 & 0 & 0.25 \\ 0.75 & 0 & 0 \\ 0 & -0.43i & 0 \end{bmatrix}. \qquad [35]$$

Because no $T_{1,2}$ relaxation is present, all states kept their population during the shift process and no longitudinal magnetization recovers either. Most importantly, an $\tilde{F}_0$ state of the population 0.75 occurs (in two complex conjugated modifications). Thus, the primary $SE_{1\text{-}2}$ of the signal intensity 0.75 is measured.

Another application of $\mathbf{S}$ and, subsequently, the second refocusing pulse $\mathbf{T_x}(120^\circ)$ leads to

$$\mathbf{\Omega}\left(t = \frac{3}{2}ESP^+\right) = \mathbf{T_x}(120^\circ)\,\mathbf{S}\,\mathbf{\Omega}(t = ESP)$$
$$= \begin{bmatrix} 0 & -0.19 & 0 & 0.06 \\ 0 & 0.94 & 0 & 0.19 \\ 0 & -0.11i & 0 & -0.11i \end{bmatrix}. \qquad [36]$$

The reader should note that operators are always sequenced from the left — they do not commute in general.

The RF pulse generated an $\tilde{F}_{-1}$ state of the population 0.94 (Fig. 12). It is a combination or sum of 0.56 from the former, partially refocused $\tilde{F}_1$ state (SE part) and 0.38 from the partially excited $\tilde{Z}_1$ state (STE part). A further shift of the transverse states by +1 leads to the set of configuration states present at the second echo time:

$$\mathbf{\Omega}(t = 2ESP) = \mathbf{S}\,\mathbf{\Omega}\left(t = \left(\frac{3}{2}ESP\right)^+\right)$$
$$= \begin{bmatrix} 0.94 & 0 & -0.19 & 0 & 0.06 \\ 0.94 & 0 & 0.19 & 0 & 0 \\ 0 & -0.11i & 0 & -0.11i & 0 \end{bmatrix}.$$
$$[37]$$

In a TSE sequence, primary SE pathways and STE pathways overlap and produce echoes at the same time due to the regular and coherent CPMG based structure. Using the suggested indexing method from the last chapter, $SE_{1\text{-}2\text{-}3}$ and $STE_{1\text{-}2\text{-}3}$ are simultaneously measured with the signal intensities 0.56 and 0.38, respectively.

Another step through the simulation of a full echo spacing with the operator sequence $\mathbf{S}\,\mathbf{T_x}(120^\circ)\,\mathbf{S}$ produces the third echo state configuration

$$\mathbf{\Omega}(t = 3ESP) = \mathbf{S}\,\mathbf{T_x}(120^\circ)\,\mathbf{S}\,\mathbf{\Omega}(t = 2ESP) =$$
$$\begin{bmatrix} 0.84 & 0 & 0.28 & 0 & -0.14 & 0 & 0.02 \\ 0.84 & 0 & -0.05 & 0 & 0.05 & 0 & 0 \\ 0 & -0.27i & 0 & -0.14i & 0 & -0.03i & 0 \end{bmatrix}.$$
$$[38]$$

As can be seen from Eq. (38), the echo intensities gradually approximate the pseudo steady state (PSS)
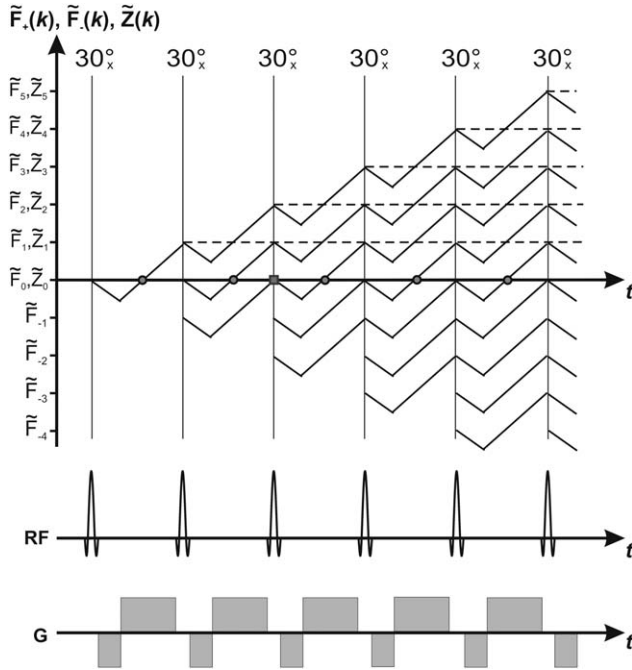
Figure 13. Extended phase diagram of a FISP, GRASS, or FAST sequence including a simplified sequence diagram of its read encoding direction. With the beginning of the third TR, all RF pulses constantly mix refocusing pathways from the previous TRs with FIDs generated from "freshly recovered" magnetization (gray square marker). This can result in a true steady state provided TR is sufficiently short compared with T_1 and T_2 (and the RF flip angles and phases satisfy particular conditions) (13,15,34,49). Directly after RF one easily counts n = 3N-2 pathways evolving for this rapid GE sequence; thus, the number of pathways grows linearly with the number of RF pulses due to the regular timing. Note that the FISP sequence uses a gradient spoiler (included in the positive lobe of the read out gradient), which actually does not spoil the transverse magnetization component: As shown, subsequent RF pulses can always refocus the magnetization (13,15,34,49).

value of $\sin(120°/2) = 0.866...$ (10). If the TSE sequence should continue, the simulation has to be equally performed for the next echo spacings.

It should be noted that EPGs for TSE sequences usually display the echo train within one repetition time TR, starting with equilibrium magnetization and, thus, suggesting something like an "eraser for magnetization" at the echo train end. This assumption often works thanks to sufficiently long TR ($T_{1,2}$ relaxation issues); yet, if TR is short compared with the relaxation times, incomplete T_1 recovery has to be considered. Additionally, T_1 recovery may be boosted by low refocusing flip angles as investigated by Weigel et al for inversion recovery prepared TSE sequences (27). A further noteworthy inter-TR effect represents residual (not T_1 relaxed) modulated longitudinal magnetization that participates every second TR in TSE signal generation as well (27).

Example: Simulating a Rapid Gradient Echo Sequence

As an advanced second step now, a rapid GE sequence will be discussed. "Rapid" means that its TR

is considerably shorter than both relaxation times. As a result, such a GE sequence necessitates relaxation and recovery effects to demonstrate true steady state behavior. Figure 13 shows the extended phase diagram of one type of rapid GE (SSFP) sequences, which uses gradient spoiling and no RF spoiling. As can be deduced from the diagram by following the pathways, this type of SSFP sequence directly reads out the FID (= $\tilde{F}_0$ state). Consequently, it is labeled as an $\tilde{F}_0$ *type* SSFP sequence and known as a FISP, GRASS, or FAST sequence (gradient spoiling but no RF spoiling) (12,13,15). The reader should note that the EPG creates a means for actually characterizing the NMR sequence here. For an in-depth discussion of this topic, the reader should study dedicated literature such as Refs. (12,13,15,60–62).

Although the given FISP sequence represents a notably different NMR sequence than the TSE sequence (Figs. 12 and 13), the procedure for simulating the FISP sequence will be very similar to that of simulating the TSE sequence from before. This underlines the flexibility and generality of the EPG concept.

Presuming a constant flip angle of 30° around the x-axis, the RF excitation pulse operator equals to (Eq. (15))

$$\mathbf{T_x}(30°) = \begin{bmatrix} 0.93 & 0.07 & -0.50i \\ 0.07 & 0.93 & 0.50i \\ -0.25i & 0.25i & 0.87 \end{bmatrix}. \qquad [39]$$

For reasons of simplicity, the $E_{1,2}$ relaxation terms will be directly defined to be $E_1 = 0.99$ and $E_2 = 0.9$ (Eqs. (23) and (24)):

$$\mathbf{E} = \begin{bmatrix} 0.90 & 0 & 0 \\ 0 & 0.90 & 0 \\ 0 & 0 & 0.99 \end{bmatrix} ;$$

$$T_1 \text{ recovery term}: \begin{bmatrix} 0 \\ 0 \\ 0.01 \end{bmatrix} \text{ for } k=0 \text{ states .} \qquad [40]$$

These parameter values roughly correspond to $T_1 = 1000$ ms and $T_2 = 100$ ms if the chosen repetition time *TR* is 10 ms.

Starting with equilibrium magnetization the initial state matrix is $\mathbf{\Omega}(t<0) = [0,0,1]^T$. At $t=0$, the excitation pulse changes the state matrix to be

$$\mathbf{\Omega}(t=0) = \mathbf{T_x}(30°)\ \mathbf{\Omega}(t<0) = \begin{bmatrix} \tilde{F}_0 \\ \tilde{F}_0^* \\ \tilde{Z}_0 \end{bmatrix} = \begin{bmatrix} -0.5i \\ 0.5i \\ 0.87 \end{bmatrix} \qquad [41]$$

It can be observed well in Eq. (41) that both $\tilde{F}_0$ states are complex conjugated partners, because the excitation pulse generates an FID of the signal intensity $-\frac{1}{2}$ on the imaginary y-axis.

If one exactly followed the extended phase or sequence diagram in regard to the simulation, a shift of all states by -1 and then by $+1$ would be necessary for mimicking the first part of the GE readout now (Fig. 13). However, the EPG concept is a pragmatic if

not a "lazy" approach: There is no need for applying both compensating gradient switches, because they have a net effect of $\Delta k = 0$ on the configuration states. Thus, the shift operator **S** will be used for the net gradient switching over the full TR, which includes the gradient spoiling moment to the end of the TR (Fig. 13) (12,13,15). Here, it may be helpful to remind the reader that the integral k of the discrete EPG approach are merely "house numbers." But what about the $\tilde{F}(0)$ state whose population represents the echo intensity of the measured GE? This population is directly calculated from the previously generated FID and its corresponding $\tilde{F}_0$ state. However, T_2/T_2^* relaxation effects have still to be considered in dependence on the selected echo time *TE*. Thus, for the short TE of a FISP sequence the first GE's signal intensity is $GE_1 = -0.50^*\exp(-TE/T_2^*) \approx -0.50^*\exp(-TE/T_2)$, if $T_2, T_2^* \gg TE$.

The next step is using the **S** operator and the relaxation operator **E** (Fig. 13):

$$\mathbf{\Omega}(t = TR^-) = \mathbf{E}\ \mathbf{S}\ \mathbf{\Omega}(t = 0) = \begin{bmatrix} 0 & -0.45i \\ 0 & 0 \\ 0.87 & 0 \end{bmatrix}. \quad [42]$$

The former FID ($= \tilde{F}_0$ state) was dephased to become an $\tilde{F}_1$ state and it also experienced T_2 decay. Additionally, the $\tilde{Z}_0$ population partially recovered. The subsequent RF pulse excites, refocuses, and stores magnetization as follows:

$$\mathbf{\Omega}(t = TR^+) = \mathbf{T_x}(30°)\ \mathbf{\Omega}(TR^-) = \begin{bmatrix} -0.43i & -0.42i \\ 0.43i & -0.03i \\ 0.75 & -0.11 \end{bmatrix}. $$
$$[43]$$

An FID of signal intensity -0.43 is generated on the y-axis, which is measured with a second GE. Its signal intensity therefore corresponds to $-0.43^*\exp(-TE/T_2)$.

Another application of the operators $\mathbf{T_x}(30°)$ **E S** on the state matrix gives

$$\mathbf{\Omega}(t = 2TR^+) = \mathbf{T_x}(30°)\ \mathbf{E}\ \mathbf{S}\ \mathbf{\Omega}(t = TR^+)$$
$$= \begin{bmatrix} -0.35i & -0.31i & -0.35i \\ 0.35i & -0.08i & -0.03i \\ 0.67 & -0.19 & -0.09 \end{bmatrix} \quad [44]$$

which represents the state matrix after two TRs.

It should be noted that the third RF pulse started to mix magnetization among "freshly recovered" and then excited magnetization and an SE generated by the first two RF pulses (gray square marker in Fig. 13). The EPG representation perfectly demonstrates that all subsequent RF pulses act similarly. This mix-in effect leads to the steady state response of the SSFP based FISP sequence (12,13,15). For this particular example, the steady state amplitude will be approximately 0.107. In contrast to TSE sequences, magnetization pathways of different history are mixed constantly (a TSE sequence has no true steady state or one could claim it is zero). Thus, echoes of complex signal weighting evolve (12,13,15).

A further note of importance is that the EPG representation in Figure 13 nicely proves that a gradient spoiler cannot *spoil* or *destroy* transverse magnetization in practice. It merely dephases it. Increasing the spoiling moment would only mean increasing the dephasing. In fact, RF pulses are always able to refocus magnetization as long as it has not decayed due to irreversible effects such as relaxation or diffusion. These effects are true "spoilers."

The next TRs of the rapid GE sequence are simulated equally. Adding RF spoiling would necessitate using a different **T** operator in every TR due to the RF phase change. For reasons of brevity, the author refrained from doing this. In a computer program, however, it would be really simple: It is a just a matter of updating the **T** matrix accordingly.

Motion Phenomena

Generally, motion phenomena such as body motion, flow or diffusion are of high importance within the field of NMR. So there is great interest in assessing their impact on the configuration states to understand quantitatively dedicated motion sensitization schemes as well as motion related artifacts. But how are the corresponding mathematical representations to be obtained?

Before dedicated motion operators within the EPG concept are discussed, it is quite helpful to understand how these operators will generally affect the configuration states. Considering the Fourier relationship between magnetization in position space and in the EPG framework, it can be learned from the Fourier shift theorem that motion phenomena will lead to phase and magnitude changes of the populations of configuration states, depending on the type of motion. This fact itself does not represent any new effect. The (basic) EPG operators investigated so far, **S**, **T**, and **E**, do the same; however, they act in a more "global" way: **S** changes the k of all present $\tilde{F}_k$ by one global Δk at a time, **T** only mixes populations in dependence on the global RF flip angle α and introduces phase shifts dependent on the global RF phase Φ, and **E** is just a time dependent global weighting factor. These three basic EPG operators do not depend on the dephasing of magnetization, i.e., they do not change the population of the configuration states in direct dependence on the state's own k. With motion effects, however, this will be different. Why is that so?

As depicted in the foundation of the EPG (Figs. 5 and 8), higher order configuration states represent more finely pitched helices and harmonic wave patterns of magnetization, and these are affected by motion in a stronger way. The configuration states carry position encoded information that is easier to destroy or alter for large spatial frequencies k, if the motion has a vector component parallel or anti-parallel to the modulation of magnetization in space. Thus, to account for this higher sensitivity to motion for large k, the motion related operators will depend on k directly, i.e., they depend on the exact k-trajectory or phase history of the isochromat ensemble (14,18,58). Thus, it is clear that all motion operators will necessitate the real k that is generated by the gradients according to Eq. (4). This necessity can require
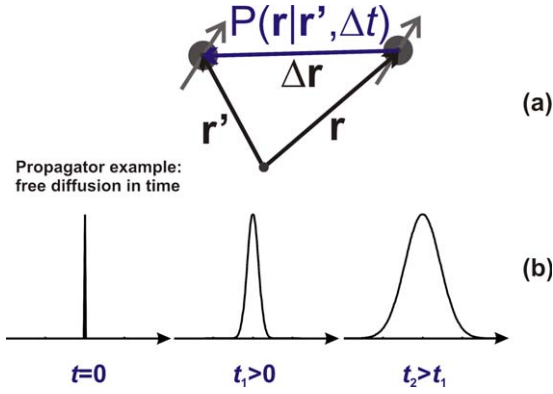
Figure 14. a: The meaning of the displacement probability $P(r|r', t)$ is displayed. As can be deduced from its name, it describes the probability that a particle or isochromat moves from the position $\mathbf{r}$ to $\mathbf{r}'$ during the time interval Δt. **b:** A typical and important example for the application of the displacement probability is the description of free diffusion. In regard to diffusion, the displacement probability is called propagator frequently. Initially, the isochromat resides at a defined position that is depicted by an infinitely narrow Gaussian, i.e., a delta distribution. Within the time the Gaussian shaped diffusion propagator broadens more and more, depicting that the isochromat will move away from its initial position most probably. Because the stochastic motion of free diffusion has no preferred direction, the propagator is symmetric. [Color figure can be viewed in the online issue, which is available at wileyonlinelibrary.com.]

considerably more effort in dependence on the complexity of the investigated MR sequence and the desired accuracy/precision of the simulation, because the exact timing of the gradient switching within the MR sequence may have to be taken into account.

A further conclusion to be made is that any k-dependent EPG operator must take different forms for transverse $\tilde{F}_\pm(k)$ and longitudinal $\tilde{Z}(k)$ states, because any active gradient will further dephase the transverse magnetization, i.e., shift the $\tilde{F}_\pm$ states, parallel to the motion effects that are depicted by the k-dependent EPG operator.

All of these effects will become more apparent in the examples below.

Motion Operators by Means of the Convolution Theorem

In the following, a general recipe for obtaining the representation of a broader class of EPG operators is derived and discussed, where the motion can be depicted using a spatially invariant displacement probability or propagator $P(\mathbf{r}|\mathbf{r}', t)$. Typical motion phenomena fulfilling this condition are rigid body motion, uniform flow in a vessel or free diffusion in a medium. These important examples are also discussed in further detail below.

The displacement probability $P(\mathbf{r}|\mathbf{r}', \Delta t)$ depicts the probability that an isochromat (or particle) will move from position $\mathbf{r}$ to position $\mathbf{r}'$ within the time Δt as shown in Figure 14a. Frequently, $P(\mathbf{r}|\mathbf{r}', \Delta t)$ is a function of $\Delta \mathbf{r} = \mathbf{r} - \mathbf{r}'$ alone, i.e., the displacement probability P is spatially invariant; it only matters how far

and in which direction the isochromat moves ($\Delta \mathbf{r}$), but not from which position exactly it starts ($\mathbf{r}$). In this case, the convolution theorem facilitates a quick solution for such motion phenomena.

In the beginning, the spatially invariant displacement probability $P(\mathbf{r}|\mathbf{r}', t)$ is known. At time $t = 0$, an arbitrary magnetization distribution $\mathbf{M}(\mathbf{r}, 0)$ is present in space. It consists of numerous isochromats that are all affected equally by the known displacement probability $P(\mathbf{r}|\mathbf{r}', \Delta t)$ (spatial invariance of P). Then, the convolution of $P(\mathbf{r}|\mathbf{r}', \Delta t)$ with $\mathbf{M}(\mathbf{r}, 0)$ leads to the motion affected magnetization in position space after the time Δt has expired (14,18):

$$\mathbf{M}(\mathbf{r}, \Delta t) = \int_V P(\mathbf{r} - \mathbf{r}', \Delta t)\, \mathbf{M}(\mathbf{r}', 0) d^3 r'. \qquad [45]$$

As a side note: The spatially invariant propagator P depicts how the magnetization $\mathbf{M}(\mathbf{r}, 0)$ will evolve with time from any given spatial point $\mathbf{r}$. Summing up all these contributions corresponds mathematically to the convolution integral given in Eq. (45) (c.f. a basic mathematical text book).

Fourier transforming Eq. (45) converts the convolution integral into a mere product in Fourier space, which corresponds to exploiting the famous convolution theorem (14,18):

$$\tilde{M}(\mathbf{k}, \Delta t) = \tilde{P}(\mathbf{k}, \Delta t) \cdot \tilde{M}(\mathbf{k}, 0). \qquad [46]$$

The last step is of great value, because Eq. (46) depicts the effect of motion on the magnetization in spatial Fourier space now. The EPG framework also depicts magnetization in spatial Fourier space (c.f. the foundation of the EPG concept above). Thus, the Fourier transforms of both magnetization distributions $\tilde{M}(\mathbf{k}, 0)$ and $\tilde{M}(\mathbf{k}, \Delta t)$ correspond directly to the initial and motion affected magnetization represented as $\tilde{F}_\pm$ and $\tilde{Z}$ states. Consequently, the Fourier transform of the displacement probability, $\tilde{P}(\mathbf{k}, \Delta t)$, is directly the EPG operator in search, which depicts the impact of such motion effects on the configuration states (14,18). This important insight will be deepened by two important examples.

Coherent Bulk Motion: Rigid Body and Uniform Flow

From a physical point of view, rigid body motion and spatially uniform flow represent phenomena of coherent macroscopic bulk motion with a given velocity $|\mathbf{v}|$ and direction $\mathbf{v}/|\mathbf{v}|$. Thus, from a qualitative point of view, it can already be understood that the whole magnetization distribution, which consists of spatial magnetization modulation patterns, will be moved coherently in space relative to the origin of our coordinate system. This coherent motion must result in phase shifts for all EPG configuration states that have $|\mathbf{k}| \neq 0$, if there is any motion component parallel or anti-parallel to the modulation pattern (Fig. 15). Hence, motion will not have any effect on the coherent $\tilde{F}_0$ and the equilibrium $\tilde{Z}_0$ state in general.

A closer look at the different orders of harmonic wave patterns in Figure 15 immediately suggests that the acquired phase shift due to coherent motion will be proportional to the dephasing $|\mathbf{k}|$ of the configuration

(a)

$\tilde{F}_+(k), \tilde{F}_-(k), \tilde{Z}(k)$

α_{n-1} α_n

$\tilde{F}_{11}, \tilde{Z}_{11}$

$\tilde{F}_9, \tilde{Z}_9$

$\tilde{F}_7, \tilde{Z}_7$

$\tilde{F}_5, \tilde{Z}_5$

$\tilde{F}_3, \tilde{Z}_3$

$\tilde{F}_1, \tilde{Z}_1$

$\tilde{F}_{-1}$

t

$\tilde{F}_{-3}$

$\tilde{F}_{-5}$

$\tilde{F}_{-7}$

$\tilde{F}_{-9}$

(b)

$M_y(z)$

(c)

object displacement

$M_y(z)$

object displacement

Figure 15. a: A part of an EPG of a TSE sequence is displayed. The secondary echo paths were omitted for reasons of overview, therefore, odd configuration states are shown only. **b:** Recalling in mind that all configuration states represent spatial harmonic patterns of magnetization, an object displacement corresponds to a global, coherent shift of all harmonic patterns in space. **c:** In this example, the object displacement equals to half a wave length of an F_1 state. As a result, the higher orders of F_3, F_5, ... acquire state dependent phase shifts of 3,5,... halves of their own wavelength. Hence, the acquired phase shift scales linearly with k and also with the object displacement, which is proportional to the object's speed.

state (14,30,39). Thus, the necessary phase adaptation directly depends on the state's own dephasing — this fact was already predicted in the general considerations made in the section before last.

The exact representation of the EPG operator for coherent macroscopic bulk motion can be obtained with the convolution approach introduced above; however, there is a simpler solution using the direct definition of **k**. The convolution approach will be used later for a validation of the result and to improve understanding.

Equation (4) defined the dephasing **k** as a spatial wave vector. It depicts the phase change per distance. This became apparent in Figure 4 where $2\pi/|\mathbf{k}|$ represented the pitch of the helix, i.e., its wave length λ in space. λ corresponds directly to the phase shift of 2π for a full period. Hence, if the object is displaced by Δx, the fraction $\Delta x/\lambda$ must be equal to the acquired phase shift $\Delta\phi$ divided by 2π (Fig. 15):

$$\frac{\Delta x}{\lambda} = \frac{\Delta\phi}{2\pi} \Rightarrow \Delta\phi = \frac{2\pi}{\lambda}\Delta x = |\mathbf{k}| \cdot \Delta x. \quad [47]$$

Presuming that the object moves with constant speed $|\mathbf{v}|$ within a time interval Δt and considering that the direction of motion $\mathbf{v}/|\mathbf{v}|$ may not be parallel to the direction of the harmonic modulation pattern $\mathbf{k}/|\mathbf{k}|$, the acquired phase change due to motion equals to

$$\Delta\phi_{\text{coherent motion}} = \frac{2\pi}{\lambda}\Delta x = \mathbf{k} \cdot \mathbf{v} \cdot \Delta t. \quad [48]$$

This phase term has to be added to the phase of a given configuration state by the coherent motion operator. This is best done by multiplying a complex phase factor of the type $\exp(-i\Delta\phi)$. In the style of the physi-

cal transport phenomenon flux, the coherent motion operator is denoted **J** and is, therefore, defined as:

$$\mathbf{J}(\mathbf{k}, \Delta t) = \exp(-i\mathbf{k} \cdot \mathbf{v} \cdot \Delta t). \quad [49]$$

This is not the final form, yet, because the approach that led to Eq. (49) presumed without saying that **k** is constant. However, for transverse $\tilde{F}$ states this will not be the case if a gradient is turned on: It will change its dephasing and, therefore, its **k** while it simultaneously acquires additional phase due to motion. Before this effect is considered, the solution of Eq. (49) will be verified by the sophisticated method provided by means of the convolution theorem discussed above.

Initially, the displacement probability $P_{\text{coherent motion}}$ is necessitated. It is represented by a delta distribution that depicts the move of an isochromat in space in dependence on time and speed (14,30)

$$P_{\text{coherent motion}}(\mathbf{r} - \mathbf{r}', \Delta t) = \delta(\mathbf{r}' - \mathbf{v} \cdot \Delta t). \quad [50]$$

Because $P_{\text{coherent motion}}$ fulfills the condition for using the convolution theorem, which was to be spatially invariant, the recipe making use of the convolution theorem can be applied. Thus, Fourier transforming Eq. (50) leads directly to

$$\tilde{P}_{\text{coherent motion}}(\mathbf{k}, \Delta t) = \exp(-i\mathbf{k} \cdot \mathbf{v} \cdot \Delta t) \equiv \mathbf{J}(\mathbf{k}, \Delta t) \quad [51]$$

which is identical to the solution found in Eq. (49).

To consider changes of **k**, the solution of Eq. (49) or Eq. (51) is presumed to be always valid for discrete but very short time intervals Δt only. Then, taking the limit

$\Delta t \to 0$ allows one to account for continuous $\mathbf{k}(t)$ trajectories (14,18,30): An integration over the scalar product in infinitesimal intervals dt is necessary. Consequently, the generalized $\mathbf{J}$ operator equals to

$$\mathbf{J}\Big(\mathbf{k}(t), \mathbf{v}, \tau\Big) = \exp\Big(-i \int_{t=0}^{\tau} \mathbf{k}(t) \cdot \mathbf{v} \; dt\Big). \qquad [52]$$

Equation (52) shows very clearly that the $\mathbf{J}$ operator depends on the precise $\mathbf{k}(t)$ trajectory, i.e., the precise switching of the gradients. In fact, this dependency was already predicted in the general thoughts in the beginning of this chapter.

The integral operator in Eq. (52) needs a scalar product between dephasing and speed, because the direction of motion relative to the direction of the spatial wave pattern does matter. Because a 1D based EPG is meant to be used, the relation $\mathbf{k} \; \mathbf{v} = |\mathbf{k}| \; |\mathbf{v}| \cos(\beta)$ will be used with β being the angle between both vectors. The simplest boundary condition for the precise $\mathbf{k}(t)$ trajectory is a constant (background) gradient (which can also be of zero amplitude). As a consequence, $\tilde{F}$ states change their dephasing linearly from $\mathbf{k}_1$ to $\mathbf{k}_2$ within the time τ in accordance with Eq. (4), whereas $\tilde{Z}$ states remain their wave vector $\mathbf{k}_1$ (14,18). Evaluating the integral operator of Eq. (52) separately for longitudinal Z states and transverse F states with the mentioned boundary conditions, leads to the two coherent motion EPG operators (14,30,39)

$$\mathbf{J}^{\mathrm{T}} = \exp\Big(-i \frac{k_1 + k_2}{2} v \; \tau \; \cos(\beta)\Big)$$
$$= \exp\Big(-i \Big(k_1 + \frac{\Delta k}{2}\Big) v \; \tau \; \cos(\beta)\Big) \qquad [53a]$$

and

$$\mathbf{J}^{\mathrm{L}} = \exp\Big(-i \; k_1 \; v \; \tau \; \cos(\beta)\Big). \qquad [53b]$$

$\mathbf{J}^{\mathrm{T}}$ is the dedicated coherent motion operator for the transverse F states, $\mathbf{J}^{\mathrm{L}}$ is the pendant for the longitudinal Z states. Finally, both representations are combined within one matrix operator

$$\mathbf{J} = \begin{bmatrix} \mathbf{J}^{\mathrm{T}} & 0 & 0 \\ 0 & (\mathbf{J}^{\mathrm{T}})^* & 0 \\ 0 & 0 & \mathbf{J}^{\mathrm{L}} \end{bmatrix}. \qquad [54]$$

The coherent motion operator of Eqs. (53) to (54) still seems to be complex, but, it should be noted that for a regular, periodic sequence $\Delta k = k_2 - k_1$ is constant, i.e., k_1 and k_2 are multiples of Δk (equally spaced EPG). Thus, by calculating Δk by means of Eq. (4), the exponential phase factors become a function of the integral values of k used in the discrete EPG approach. Then, they are included in the framework similar to the others operators.

By considering the speed as a function of time, $\mathbf{v} = \mathbf{v}(t)$ in Eq. (52), flow or motion phenomena of higher order in t such as acceleration can also be described quantitatively. It is a matter of appropriately evaluating the integral alone.

The coherence property of the presumed motion so far, does not result in any attenuation of the configu-

ration states' populations. However, this will be different for the next example: diffusion.

Incoherent Motion: Free Isotropic Diffusion

Diffusion effects in NMR have been studied for a long time due to permanent scientific and clinical interest. Thus, there are several publications that deal quantitatively with diffusion effects. Because diffusion problems are frequently solved in Fourier space, these solutions can often be applied within the EPG calculus (2,8,9,14,16–18,30,53,54,63–65).

The most general EPG solution in regard to diffusion was published by Weigel et al (18). It considers anisotropic diffusion in 3D space and NMR sequences with arbitrary gradient shapes and directions as well as nonperiodic time intervals. Discussing the topic in this generality is beyond the scope of this work, however, the concepts discussed above will considerably aid in the process of discussing 1D isotropic free diffusion with the diffusion coefficient D.

Before the appropriate calculations are discussed, Figure 16 is meant to give a notion what will happen to the configuration states within the EPG framework. This pictorial presentation was suggested by Scheffler in an educational talk of the European Society for Magnetic Resonance in Medicine and Biology (ESMRMB) several years ago. Because there is no net bulk motion of the whole isochromat ensemble, no net phase shifts will occur for the $\tilde{F}$ and $\tilde{Z}$ states. Contrary, due to the stochastic nature of the diffusional motion, each isochromat acquires an individual phase shift which leads to a blurring of the magnetization patterns in space (c.f. diffusion propagator in Fig. 14b). This destruction of the harmonic wave patterns results in the decay of macroscopic magnetization and is equivalent to the attenuation of the populations of the configuration states. Thus, the diffusion operator will diminish EPG populations and this effect will be significantly stronger for states of higher order k (Fig. 16).

Starting with the common propagator for isotropic free diffusion in 1D (c.f. graphical sketch in Fig. 14b) (2,8,9,14,16–18,30,53,54,63–65)

$$P(r, \Delta t) = \frac{1}{\sqrt{(4\pi \; D \; \Delta t)}} \exp\Big(-\frac{r^2}{4D\Delta t}\Big) \qquad [55]$$

the convolution approach will be used immediately (Eqs. (45) and (46)) to obtain its Fourier representation and, thus, the EPG operator

$$\tilde{P}(k, \Delta t) = \exp(-Dk^2 \Delta t) \; . \qquad [56]$$

It should already be noted that the diffusion operator in Eq. (56) represents a population attenuating operator that depends on the square of k. Thus, higher order configuration states will be considerably more sensitive to the diffusional motion, which is in accordance with Figure 16.

In an equivalent way to before, the limit $\Delta t \to 0$ of the former discrete time interval allows one to account for continuous k-space trajectories and define the EPG diffusion operator $\mathbf{D}$ for isotropic diffusion (14,17–19):
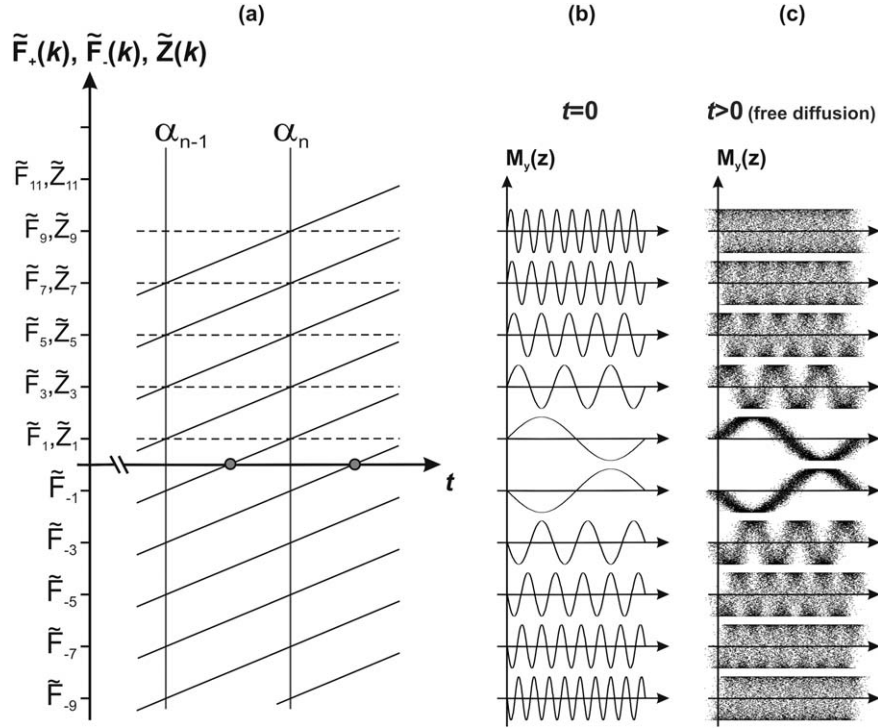
Figure 16. A part of an EPG of a TSE sequence is displayed. **a:** The secondary echo paths were omitted for reasons of overview, therefore, odd configuration states are shown only. All configuration states representing spatial harmonic patterns of magnetization (**b**) are affected by the incoherent diffusional motion of the isochromats (**c**). All EPG states with $k \neq 0$ represent information that is destroyed due to the stochastic nature of diffusion. This results in a diffusion induced damping term. As can be observed well, states of higher spatial frequency k are considerably more affected than of low modulation frequency. In fact, the diffusion sensitivity is proportional to k^2. The pictorial explanation in (c) was suggested and presented by Klaus Scheffler in an educational talk of the European Society of Magnetic Resonance in Medicine and Biology (ESMRMB) several years ago.

$$\mathbf{D}_{1D}\left(k(t), D, \tau\right) = \exp(-b_\tau D) \text{ with } b_\tau = \int_{t=0}^{\tau} k^2(t)dt.$$

[57]

The result of the isotropic diffusion operator, Eq. (57), was expressed in terms of the well-known diffusion weighting term $\exp(-bD)$ (18,66,67). The significant difference, however, is that the defined b-factor in Eq. (57) depends on each investigated configuration state and pathway due to the $k(t)$ dependence (2,8,9,14,16–19,30,53,54,63–65). Consequently, multi-RF pulse sequences such as TSE or types of SSFP will exhibit a rather complicated diffusion sensitivity (18,19,58,68,69).

As a side note, the b-factor in Eq. (57) consists of an integral that corresponds to solids of revolution. Ref. (18) gives an interesting graphical interpretation of this observation.

Finally, the diffusion integral operator from Eq. (57) is evaluated for the boundary condition of a constant (background) gradient. This is done in the same way as for the coherent motion operator discussed above. As a result, the two dedicated isotropic diffusion operators correspond to (2,8,9,14,16–19,30,53,54,63–65)

$$\mathbf{D}_{1D}^T = \exp(-b_\tau^T D)$$

$$\text{with} \quad b_\tau^T = (k_1 + k_2)^2 \frac{\tau}{4} + (k_1 - k_2)^2 \frac{\tau}{12}$$

[58a]

$$= \left(k_1 + \frac{\Delta k}{2}\right)^2 \tau + \frac{(\Delta k)^2}{12}\tau$$

$$\mathbf{D}_{1D}^L = \exp(-b_\tau^L D) \text{ with } b_\tau^L = (k_1)^2 \ \tau \ .$$

[58b]

$\mathbf{D}_{1D}^T$ is the dedicated free diffusion operator for the transverse $\tilde{F}$ states, $\mathbf{D}_{1D}^L$ is the pendant for the longitudinal $\tilde{Z}$ states. Finally, both representations are combined within one matrix operator

$$\mathbf{D}_{1D} = \begin{bmatrix} \mathbf{D}^T & 0 & 0 \\ 0 & \mathbf{D}^T & 0 \\ 0 & 0 & \mathbf{D}^L \end{bmatrix}.$$

[59]

The diffusion operator with its state/pathway specific b-factor (Eqs. (58) to (59)) seems to be rather complex; but, using the same argument from above, in a regular, periodic sequence $\Delta k = k_2 - k_1$ is constant, i.e., k_1 and k_2 are multiples of Δk (equally spaced EPG). Thus, by calculating Δk by means of Eq. (4), the exponential decay terms become a function of the integral values of k used in the discrete EPG approach. Then, they are included in the framework similar to the others operators. The reader may check on the EPG software the author provides to validate this (c.f. chapter coding).

Equations (58) and (59) facilitate determining quantitative diffusion sensitivity in multi-pulse sequences and diffusion preparations, among them different types of SSFP sequences, long echo train TSE sequences with varying flip angles, and superstimulated diffusion preparation schemes (38,43,58,70). For clinical applications, assessing an effective b-factor based on the EPG concept has proven valuable (58).

Extensions, Limitations, and Software Coding

It has been shown that the EPG is a very useful concept for depicting MR sequences for a broad range of applications. In recent years a broader theoretical understanding of the EPG concept has been achieved and further extensions of the concept have been developed. This last chapter explains additional extensions, possibilities, and applications, besides linking the topic to adjacent NMR techniques. Furthermore, the limitations are discussed and some worthwhile notes about the software coding are presented, including the availability of "ready-made" software.

So far, all descriptions and applications presented within this review presumed that the flip angle(s) of the RF pulses are known a priori. Hence, starting from a given initial magnetization or configuration vector, all configuration states are calculated successively over time. Particularly, all occurring $\tilde{F}_0$ states are quantified, representing the generated echoes and their intensities. However, Hennig et al. demonstrated that the EPG concept also facilitates the solution of the much more complex "inverse calculation" (23). The "inverse calculation" or "inverse problem" means that the RF flip angles (and possibly RF phases) are unknown. On the contrary, all echo intensities throughout an echo train are initially defined; or a targeted set of configuration states from an NMR sequence is given a priori. Then, starting with a given magnetization constellation, what are the exact RF flip angles needed to generate these targeted echo intensities or configuration states (23)? This challenge is of great interest in practice, because the various echoes and their intensities have a direct impact on the later image properties such as signal intensities of tissue, contrasts between different tissues and point spread function(s) (PSF) (47). Thus, in predefining such characteristic image and/or tissue properties, the EPG concept facilitates this inverse calculation to determine the appropriate set of flip angles needed. For instance, several publications have made use of this possibility for TSE sequences with dedicated varying flip angle schemes in recent years (23,27,29,31,39–42,56). Apart from a full sequence design, this method can also be used to prepare specific magnetization configurations (38).

Whereas for the forward calculation with known RF flip angles and phases, the results for the echo intensities are unique, this is not true for the inverse calculation: Depending on the parameter constraints of the problem, the number of possible flip angle solutions can be infinite (!). This "bold statement" can be verified using a short example: From the **T** operator matrix (Eq. (15)), it can be seen that the relative intensity of a single spin echo equals to $\sin^2(\alpha/2)$. What refocusing flip angle would be needed to refocus $1/4 = 25\%$? Solving the equation for α immediately shows that already two solutions $\alpha_{1,2} = \pm 60°$ are possible. However, both flip angle solutions are still modulo $360°$. Furthermore, the phases of both magnetization and RF pulses were still neglected, which would become important if multi-pulse experiments are regarded, because the generated EPG pathways would
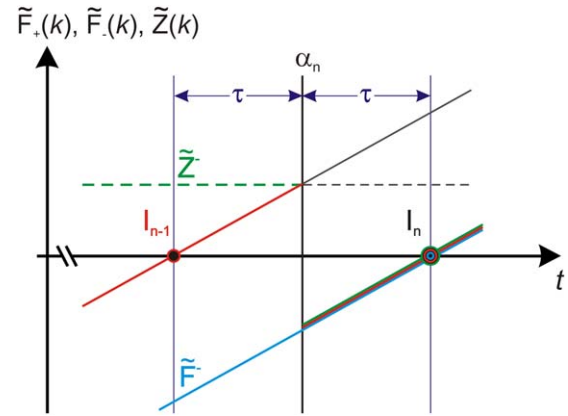

Figure 17. The part of an EPG is presented demonstrating how the inverse calculation works. In the most general case of a regular and periodic NMR sequence the RF pulse of unknown flip angle generates an echo from partially refocusing the previous echo (SE), partially exciting modulated z-magnetization (STE), and partially leaving rephasing magnetization unaffected. By initially solving the **T** operator for the flip angle, it can be determined based on the previous state populations to generate the desired echo intensity. [Color figure can be viewed in the online issue, which is available at wileyonlinelibrary.com.]

interfere differently, thus leading to different populations and, eventually, different echo intensities.

The simplest method of EPG based "inverse calculation" is the so called "1-ahead algorithm" as illustrated in Figure 17 (23). In the following, all configuration states and the used RF pulse are meant to have the same phase $\varphi = \Phi = 0°$. One interval within a regular and periodic NMR sequence is investigated that represents the most general case, because different coherence paths from transverse $\tilde{F}_\pm$ and longitudinal $\tilde{Z}$ states will overlap to produce the targeted echo (Fig. 17). In this case, RF pulse #n, which generates echo #n of intensity I_n, superposes fractions of three different pathways from interval n-1: It partially refocuses echo #n-1 of intensity I_{n-1}, it partially stimulates z-magnetization and it partially mixes in rephasing magnetization of interval (n-1) (higher order echo) (23), Figure 17. The fractions directly depend on the flip angle α_n as depicted by **T** (Eq. (15)). Writing out this relation including $T_{1,2}$ relaxation gives (Fig. 17):

$$\frac{I_n}{E_2} = E_2 \cdot \sin^2\left(\frac{\alpha_n}{2}\right) \cdot I_{n-1} + E_2 \cdot \cos^2\left(\frac{\alpha_n}{2}\right) \cdot \tilde{F}^- + i \cdot E_1 \cdot \sin(\alpha_n) \cdot \tilde{Z}^-.$$

$$[60]$$

Equation (60) uses the $E_{1,2}$ relaxation terms introduced in Eq. (23). Please note that the general complex **T** operator with $\Phi = 0$ from Eq. (15) was used here, whereas Hennig et al used the special $\mathbf{T}_{CMPG}$ operator from Eq. (21).

Equation (60) can be analytically solved for the desired flip angle α_n if the appropriate trigonometric relations are used, which express the whole equation in terms of $\tan(\alpha_n/2)$: $\sin^2\alpha = \frac{\tan^2(\alpha)}{1+\tan^2(\alpha)}$, $\cos^2\alpha = \frac{1}{1+\tan^2(\alpha)}$,

and $\sin 2\alpha = \frac{2\tan(\alpha)}{1+\tan^2(\alpha)}$. Thus, solving Eq. (60) for $\alpha_n = \alpha(n)$ leads to the two solutions

$$\alpha_{1,2}(n) = 2\arctan$$

$$\left(\frac{-iE_1 E_2 Z^- \pm \sqrt{-E_1^2 E_2^2 (Z^-)^2 - (E_2^2 F^- - I_n)(E_2^2 I_{n-1} - I_n)}}{E_2^2 I_{n-1} - I_n} \right).$$

[61a]

The redefinition $\tilde{Z}^- \rightarrow i \cdot \tilde{Z}^-$ as well as the relations $i^2 = -1$ and $(i Z^-)^2 = -(\tilde{Z}^-)^2$ give the solution for the real CPMG based EPG using the special $\mathbf{T}_{\mathrm{CMPG}}$ operator from Eq. (21):

Real CPMG:

$$\alpha_{1,2}(n) = 2\arctan$$

$$\left(\frac{E_1 E_2 Z^- \pm \sqrt{E_1^2 E_2^2 (Z^-)^2 - (E_2^2 F^- - I_n)(E_2^2 I_{n-1} - I_n)}}{E_2^2 I_{n-1} - I_n} \right).$$

[61b]

It should be noted that Eq. (61b) does not completely agree with Hennig's original solution (23), because he started the calculations with an erroneous $\mathbf{T}_{\mathrm{CMPG}}$ operator (c.f. section "Real Valued Representations within the EPG").

Now, the full recipe is to start with the desired intensities $I_1 \ldots I_N$ from a given initial magnetization configuration; e.g., "freshly excited" x-magnetization $\tilde{F}_0 = I_0 = 1$. The first flip angle necessitated is calculated by means of Eq. (61a) or Eq. (61b) to get the first desired echo intensity I_1 ("1-ahead inverse calculation") (23). Because two solutions result, the one with the lower flip angle should be used due to a lower RF power deposition and specific absorption rate (SAR) (23). Then, taking the flip angle just calculated, the EPG is computed *forward* to get all current EPG states. This is significant because the residual, higher order states may become important in later intervals. Then, the second flip angle solution is calculated inversely by means of Eq. (61a) again, the lower flip angle from both solutions being taken that produces the second echo intensity I_2, and so on successively — until all desired flip angles are known (23). Ref. (23) also depicts the more sophisticated EPG based techniques for solving the inverse calculation, the "2-ahead algorithm" and the "3-ahead algorithm."

Equations (13a) to (13c) defined the fundamental basis for the EPG concept. They represent a quite general basis in 3D Fourier and spatial space (18). However, due to the effectiveness of the 1D-dephasing approach within the EPG concept, the literature almost exclusively deals with this type of EPGs (10–17,23–29). For a complete 3D EPG concept, $\mathbf{k}$ can be defined component-wise by means of $k_n(t) = \gamma \int_{t'=0}^{t} G_n(t')\, dt'$, where $n = $ x,y,z or any other orientation of an orthogonal gradient system (18). Then, all configuration states will depend on a full dephasing vector $\mathbf{k}$: $\tilde{F}_{\mathbf{k}}$ and $\tilde{Z}_{\mathbf{k}}$. Among the applications are MR sequences with three simultaneous encoding axes and the quantification of anisotropic diffusion effects, i.e., a 3D anisotropic diffusion operator, as shown by

Weigel et al (18). Important to note is that with the change to a 3D reference system, one very practical property of the scalar k, which becomes the vector $\mathbf{k}$, is lost: Vectors do not have a sign; thus, the very practical sign based distinction of a transverse $\tilde{F}$ state with $k > 0$ being dephased and with $k < 0$ being rephasing is lost. This is logical, because an arbitrary vector $\mathbf{k}$ will, generally, represent superpositions of dephasing and rephasing transverse magnetization along different dephasing axes.

The fundamental basis from Eqs. (13a) to (13c) also allows for fractional, nonintegral values of k in nonequidistant steps. Indeed, this is of practical interest, because it facilitates the simulation of EPGs of magnetization preparation modules, for example, or of a nonequidistant EPG as was discussed in Figure 11. Due to the presence of several different gradients, such an EPG approach becomes essential if the exact diffusion sensitivity of an MRI sequence is meant to be assessed. Weigel and Hennig proved the feasibility by assessing the inherent diffusion sensitivity in terms of effective b-factors per encoding axis for different TSE sequences (58).

Recently, the EPG framework was extended to a spatially resolved variant (SR-EPG) by Malik et al (71). In this sophisticated EPG approach, the RF flip angle and its phase ($\mathbf{T}$ operator) as well as the tissue's relaxation times ($\mathbf{E}$ operator) become spatially dependent to allow for rapid voxel-based signal estimations under inhomogeneity conditions (71). SR-EPGs were used successfully with parallel transmission to facilitate dynamic RF shimming over a whole RF pulse train in probes and in vivo (71).

Generally, the EPG concept represents a stepwise or sequential method: To quantify the 100th echo of a common TSE sequence, the full EPG over the previous 99 echoes has to be quantified before. In this respect the EPG does not differ from a Bloch simulation that is performed in successive, discrete time intervals. However, Lukzen et al. demonstrated that analytical expressions for the configuration states of, particularly, periodic RF pulse train sequences such as CPMG and FLASH are feasible (24,28). "Analytical expressions" means that an equation can be found that directly expresses the intensity of echo #n in a closed form. Specifically, the echo amplitudes of multiple spin echo sequences are represented by sums of Legendre polynomials (24,28) if relaxation is neglected. But, it should be noted that these analytical expressions still consist of series, i.e., sums of different mathematical terms, that are of the order n with n being the echo number (24,28). Hence, the length and complexity of the solutions increase with echo number n. Motion effects like diffusion cannot be considered (24,28).

Further analytical developments are related to the improved theoretical depiction of RF spoiling as published by Ganter (25,26). Based on this expanded EPG approach, Ganter was able to derive an analytical solution for the transient response of steady-state free precession sequences (25,26).

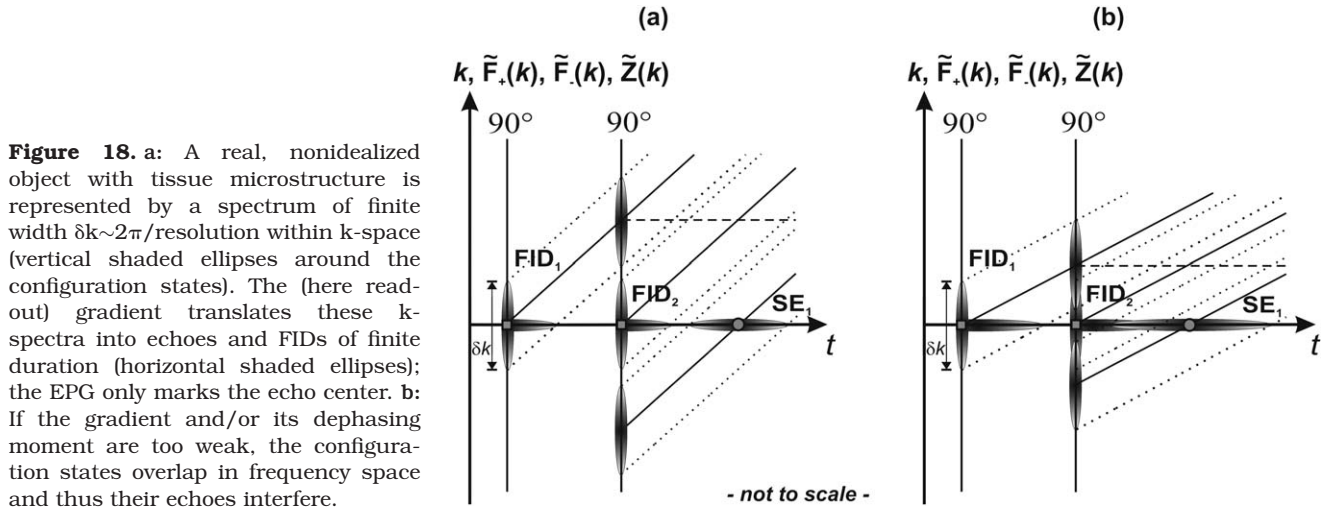Beyond the quantitative and pictorial description of imaging sequences, the EPG concept can be used to

Figure 18. a: A real, nonidealized object with tissue microstructure is represented by a spectrum of finite width $\delta k \sim 2\pi$/resolution within k-space (vertical shaded ellipses around the configuration states). The (here readout) gradient translates these k-spectra into echoes and FIDs of finite duration (horizontal shaded ellipses); the EPG only marks the echo center. **b:** If the gradient and/or its dephasing moment are too weak, the configuration states overlap in frequency space and thus their echoes interfere.

generate or "imprint" specific magnetization patterns in a medium. This approach works very well, because configuration states represent harmonic wave patterns of longitudinal and transverse magnetization in space — as was thoroughly discussed in this review. But, any desired pattern can be approximated by a sum of harmonic waves, which is what the EPG exactly represents regarding magnetization. So, to put it briefly, Fourier transforming a desired magnetization pattern leads directly to its EPG representation in terms of populations of configuration states. These EPG populations have to be generated by a combination of gradients and RF pulses, a possible magnetization preparation module. And targeting particular EPG populations can be achieved with the "inverse calculation" depicted above (23). In fact, the whole procedure can be regarded as a Fourier synthesis. Hennig et al exploited such a concept to improve the signal efficiency of the basic stimulated echo sequence to produce so called superstimulated echoes (38).

It is also valuable to see the similarities between the EPG concept and other concepts; one example would be the shaping of soft RF pulses with the Shinnar-Le Roux algorithm (16,47,72), another manner of signal synthesis.

Sadly, all these theoretical concepts are beyond the scope of this review and cannot be discussed in further detail, yet are mentioned to provide a broader overview of the subject.

The EPG concept does also have limitations and prerequisites; however, these are often discussed only briefly or not mentioned or considered at all. Within the EPG framework, RF pulses are usually treated as delta peaks, i.e., instantaneous rotations within a homogenous object. Any effects of off-resonance, line shapes, relaxation or diffusion during finite-duration RF pulses are therefore neglected (*hard pulse approximation*) (47)). For simulations, a convenient improvement consists of allocating to RF pulses a given duration where gradients, relaxation, and diffusion are considered. The instantaneous rotation takes place at the isodelay of the RF pulse (58). More sophisticated solutions for shaped soft RF pulses

could be incorporated using a DANTE-like approach (14,30,50,51).

Equivalent to the Bloch equation (8), the EPG concept presumes an uncoupled spin $1/2$ spin system, of which the EPG actually is a complex Fourier representation. Possible ways to include coupling effects are demonstrated by Sodickson and Cory (14).

When working with EPGs and SR-EPGs in particular (see above), it has to be kept in mind that, actually, voxel are not cuboid in shape. Thus, treating each voxel as independent like in the SR-EPG approach (71), is directly connected to a general EPG postulate suggested: All configuration states except for $\tilde{F}_0$ shall not contribute any signal, i.e., are properly dephased (11,15) (Figs. 7 and 8). This is one of the major reasons that EPG literature commonly decomposes magnetization into discrete Fourier series and depicts magnetization by means of configuration states of multiples of linear 2π dephasing per voxel or per object (10–17,23–29). Indeed, this postulate is true for most MR imaging and spectroscopy sequences, however, only under highly idealized conditions! The strict assumption is that the object is homogeneous in the dephasing coordinate direction – at least per voxel – such that it corresponds to a delta peak in spatial frequency space (private discussion with V. Kiselev and J. Leupold, Freiburg, Germany and C. Ganter, Munich, Germany). In fact, an object or medium of finite spatial extension with tissue microstructure, susceptibility effects and different diffusion coefficients is imaged. Thus, the object or medium is represented by a continuous spectrum of finite, approximate width of $\delta k \sim 2\pi$/resolution in frequency space. This results in a broadening of the EPG states and pathways, as illustrated in Figure 18 in a pictorial way. Thus, it is deduced that all configuration states except for $\tilde{F}_0$ have to be *sufficiently dephased* at a given time of data acquisition, which is equivalent to saying that MR spoiler, crusher, diffusion, and other gradients of a *minimal moment* are needed to lead to a correct description with such approximated EPGs (Fig. 18). This observation is also in direct accordance with investigations by Leupold et al,
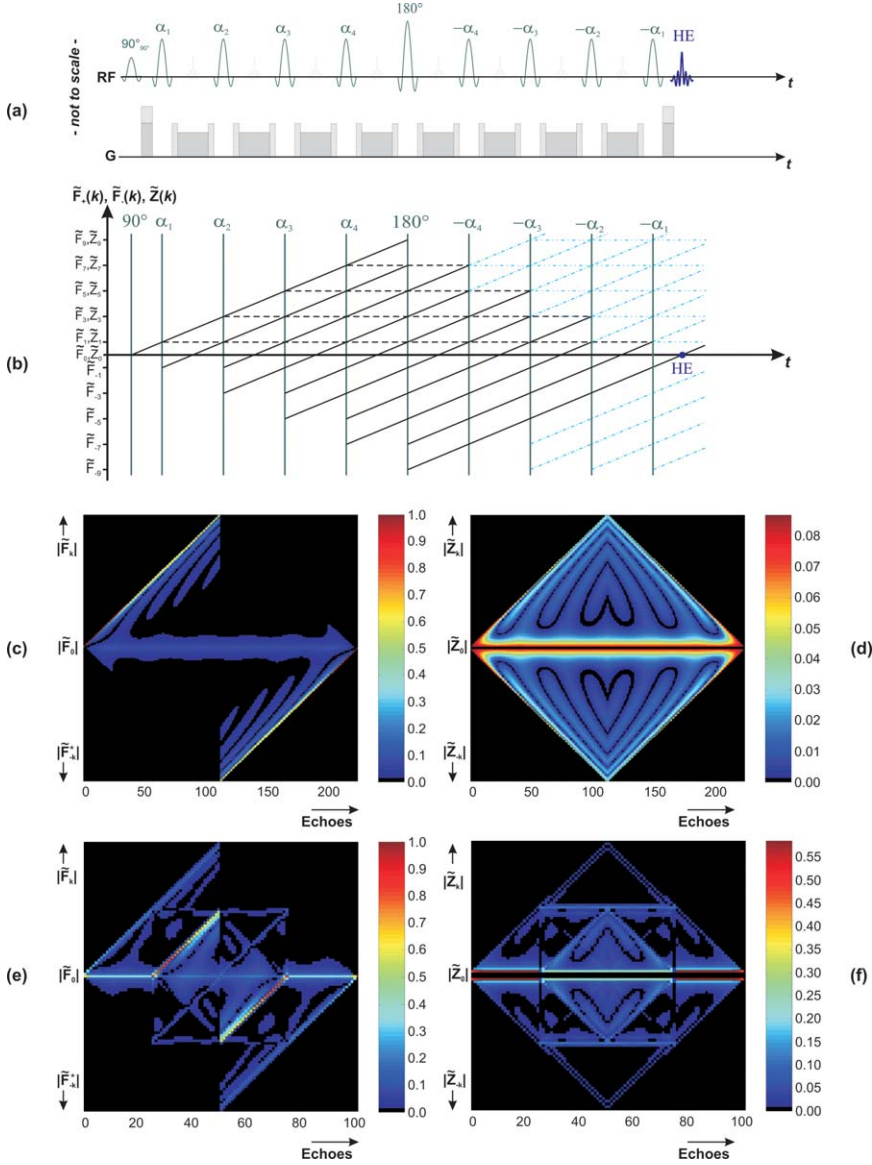
Figure 19. a: Sequence diagram of a CPMG sequence that makes use of the Hyperecho mechanism with its anti-symmetric flip angle structure. At the end of this sequence all magnetization is refocused to generate the Hyperecho (HE). **b:** The corresponding effective EPG of the Hyperecho sequence is displayed. In this respect "effective" means that all vanishing longitudinal and transverse pathways have blue instead of black color and a different line style than usual, thus, it is easier to observe the symmetric structure with respect to the vertical line representing the $180°$ refocusing pulse. The final $\tilde{F}_0$ state equals to the HE. **c,d:** Color display of the transverse (c) and longitudinal (d) state evolution matrix (Eqs. (27a) and (27b)) of such a Hyperecho sequence with 223 refocusing pulses of constant $10°$ flip angle. The state evolution diagrams clearly reflect the symmetry and that all magnetization is refocused completely to become a HE of signal intensity 1. **e,f:** The same representation for a Hyperecho sequence with 101 refocusing pulses using a more sophisticated flip angle scheme.

which conclude that the mandatory 2π spoiler gradient in RF spoiled gradient echo imaging neither is justified nor can be fulfilled for real experiments (73). Hennig intentionally used such an effect for letting echoes mutually interfere in his "MR interferography" (74). In practice, the minimal dephasing moment per TR, ESP, or equivalent period depends on the object or medium.

After the detailed discussion of the EPG concept, it seems to be rather straightforward to program a matrix operator based framework like the EPG into a computer. However, experience tells that people rather often fail nevertheless. In addition to obvious programming errors—according to the experience of the author—one common stumbling block is that the $\tilde{F}_0$ state exists in the two complex conjugated modifications $\tilde{F}_+(0)$ and $\tilde{F}_-(0)$. Neglecting this effect leads to the failure of the framework. In direct connection with this fact are the two complex conjugated transverse bases $\tilde{F}_+$ and $\tilde{F}_-$. Based on the discussion of the symmetry relations (Eqs. (13a) and (13b)) and in the chapter "Graphical Representation: Extended Phase Diagrams," the half of both bases is redundant. This fact alone would not pose a problem; however as so to put it, RF pulses (**T** operator) and gradients (**S** operator) work in two different "natural" domains of these bases: The **T**-operator exchanges populations among the domains $\tilde{F}_+(+k)$ and $\tilde{F}_-(-k)$ (or $\tilde{F}_+(-k)$ and $\tilde{F}_-(+k)$). This operation includes a complex conjugation of the population of a given configuration state besides the inversion of its k. The S operator merely changes k in the domain of the given state. This effect becomes of eminent importance if the state is shifted across $k = 0$, i.e., the $\tilde{F}(0)$ state, because its population does not experience the complex conjugation. A short example: Given a state $\tilde{F}_+(+2)$, a $180°$ RF pulse will convert it into an $\tilde{F}_-(-2)$ state. The resulting net change in dephasing therefore is $\Delta k = -4$. By contrast, a shift operator $S(\Delta k = -4)$ acting on the given $\tilde{F}_+(+2)$ state leads to an $\tilde{F}_+(-2)$ state, thus, they are not the same.

The solution to this challenge is to initially decide with which domains the programmer wants to work. If

the programmer decides working with both $\tilde{F}_+$ and $\tilde{F}_-$, the populations of the configuration states have to be complex conjugated when these are shifted across the coherent $\tilde{F}(0)$ state. Basically, this procedure corresponds to an exchange between the two modifications $\tilde{F}_+(0)$ and $\tilde{F}_-(0)$. Based on a comment about the necessity for a complex conjugate operation for $k = 0$ transitions, it appears that Malik et al used such an approach for the SR-EPG concept (71). If the programmer decides for either the full $\tilde{F}_+(\pm k)$ or the full $\tilde{F}_-(\pm k)$ domain, the **T** operator has to be modified accounting for that. The advantage of this approach is that $k = 0$ transitions do not matter and only one $\tilde{F}(0)$ state exists. For reasons of consistency in regard to the **T** operator, the presented examples use the first approach (c.f. chapter "Examples for MRI Sequences").

To make the manuscript complete, the author provides two representative EPG code implementations, which can be downloaded from http://epg.matthias-weigel.net/ or just email the author. Both codes are complementary in timing, data handling and mathematical representation: (i) an SSFP code similar to Ref. (15), yet with complex basis, RF spoiling (34), and a simple diffusion operator; (ii) a combined CP/CPMG (TSE) simulator with real basis and compact configuration state data storage. This code does include a simple diffusion operator as well.

Regarding further ready to use software, Scheffler was the first to publish an EPG coding for SSFP based sequences at all (15). Hargreaves provides code for simulating EPGs of different sequences which can be downloaded from http://bmr.stanford.edu/epg/ (19). Furthermore, Weigel et al suggested a more general approach for simulating EPGs with nonregular timing and dephasing (18); more information about his software framework "*EPGspace*" can be found on his Web page http://epg.matthias-weigel.net/.

Finally, as a neat and helpful method, the author suggests and recommends the simulation of a Hyperecho based NMR sequence (75) as an excellent test for the validity of EPG software coding. Without considering any magnetization decay from relaxation, diffusion, and flow, the Hyperecho mechanism ensures perfect refocusing for the last echo, provided that the Hyperecho symmetry relations for the RF flip angles and phases and for the dephasing intervals are maintained (75). The mechanism's response is identical to a perfect $180°$ refocusing pulse, although an arbitrary number of RF pulses with arbitrary flip angles and phases can be used (75). Thus, any loss of signal intensity, split or unexpected phase change of the final configuration state must be due to a major flaw in the programmed EPG framework (if the Hyperecho sequence is valid). The final configuration state has to be an $\tilde{F}_0$ state with the population of magnitude 1 and the same phase as a conventional, single SE would produce (75).

Figure 19a depicts a representative example for a relatively short Hyperecho mechanism implemented in a common CPMG sequence. The corresponding EPG is displayed in Figure 19b. Such a Hyperecho sequence therefore considerably tests the functions of dephasing, RF pulses and recombination/superposi-

tion of different configuration states within the software. A shift of all RF phases (including the $90°$ excitation pulse) by $\pm 90°$ will even test if the programmer has taken good care of correct complex conjugating between the $\tilde{F}_+$ and $\tilde{F}_-$ states, because magnetization is then excited on the imaginary y-axis (initially $\tilde{F}_0 = \pm i$, see above).

Particularly for sequences consisting of dozens of RF pulses, the Hyperecho mechanism also represents a very sensitive test in regard to the accuracy and precision of the calculated results, the source for deviations being quantization errors: It is sufficient to subtract 1 from the final $\tilde{F}_0$ population.

Figure 19c–f shows the results of two representative Hyperecho sequence simulations in terms of state evolution diagrams (Eqs. (27a) and (27b)). The symmetry structure mirrored in the state populations with the inversion of the central $180°$ refocusing pulse can be observed excellently.

And as a final point, Figure 19 also demonstrates very well that EPGs can even produce some modest art.

CONCLUSION

The EPG concept represents a powerful tool for depicting and understanding magnetization response of several MRI and MRS sequences. It allows pictorial understanding of echo generation, simple but elegant classification of echoes, and at the same time fast and accurate computation of echo intensities. It particularly demonstrates its advantages in the application for NMR sequences with multiple gradients and RF pulses. Motion effects such as rigid body motion, flow or free diffusion can be considered as well. All in all, the EPG is a concept that is really worth studying particularly for, but not limited to, physicists, engineers, and users who want to get a deeper insight into the understanding and development of (modern) complex NMR sequences.

REFERENCES

1. Hahn EL. Spin echoes. Phys Rev 1950;80:580–594.
2. Carr HY, Purcell EM. Effects of diffusion on free precession in nuclear magnetic resonance experiments. Phys Rev 1954;94:630–638.
3. Meiboom S, Gill D. Modified spin-echo method for measuring nuclear relaxation times. Rev Sci Instrum 1958;29:688–691.
4. Hennig J, Nauerth A, Friedburg H. RARE imaging: a fast imaging method for clinical MR. Magn Reson Med 1986;3:823–833.
5. Hore J. Solvent suppression in Fourier transform nuclear magnetic resonance. J Magn Reson 1983;55:283–300.
6. Bloch F. Nuclear induction. Phys Rev 1946;70:460–474.

7. Jaynes ET. Matrix treatment of nuclear induction. Phys Rev 1955;98:1099–1105.

8. Woessner DE. Effects of diffusion in nuclear magnetic resonance spin-echo experiments. J Chem Phys 1961;34:2057–2061.

9. Kaiser R, Bartholdi E, Ernst RR. Diffusion and field-gradient effects in NMR Fourier spectroscopy. J Chem Phys 1974;60:2966–2979.

10. Hennig J. Multiecho imaging sequences with low refocusing flip angles. J Magn Reson 1988;78:397–407.

11. Hennig J. Echoes - how to generate, recognize, use or avoid them in MR-imaging sequences. Part I. Concepts Magn Reson 1991;3:125–143.

12. Hennig J. Echoes - how to generate, recognize, use or avoid them in MR-imaging sequences. Part II. Concepts Magn Reson 1991;3:179–192.

13. Sobol WT, Gauntt DM. On the stationary states in gradient echo imaging. J Magn Reson Imaging 1996;6:384–398.

14. Sodickson A, Cory DG. A generalized k-space formalism for treating the spatial aspects of a variety of NMR experiments. Prog Nucl Magn Reson Sp 1998;33:77–108.

15. Scheffler K. A pictorial description of steady-states in rapid magnetic resonance imaging. Concepts Magn Reson 1999;11:291–304.

16. Vlaardingerbroek MT, den Boer JA. Magnetic resonance imaging. Berlin: Springer Verlag; 2004.

17. Zur Y. An algorithm to calculate the NMR signal of a multi spin-echo sequence with relaxation and spin-diffusion. J Magn Reson 2004;171:97–106.

18. Weigel M, Schwenk S, Kiselev VG, Scheffler K, Hennig J. Extended phase graphs with anisotropic diffusion. J Magn Reson 2010;205:276–285.

19. Hargreaves BA, Miller KL. Using extended phase graphs: review and examples. In: Proceedings of the 21st Annual Meeting of ISMRM, Salt Lake City, 2013. (abstract 3718).

20. Rabi II, Ramsey NF, Schwinger J. Use of rotating coordinates in magnetic resonance problems. Rev Mod Phys 1954;26:167–171.

21. Ljunggren S. A simple graphical representation of Fourier-based imaging methods. J Magn Reson 1983;54:338–343.

22. Twieg DB. The k-trajectory formulation of the NMR imaging process with applications in analysis and synthesis of imaging methods. Med Phys 1983;10:610–621.

23. Hennig J, Weigel M, Scheffler K. Calculation of flip angles for echo trains with predefined amplitudes with the extended phase graph (EPG)-algorithm: principles and applications to hyperecho and TRAPS sequences. Magn Reson Med 2004;51:68–80.

24. Lukzen NN, Savelov AA. Analytical derivation of multiple spin echo amplitudes with arbitrary refocusing angle. J Magn Reson 2007;185:71–76.

25. Ganter C. Steady state of gradient echo sequences with radiofrequency phase cycling: analytical solution, contrast enhancement with partial spoiling. Magn Reson Med 2006;55:98–107.

26. Ganter C. Analytical solution to the transient phase of steady-state free precession sequences. Magn Reson Med 2009;62:149–164.

27. Weigel M, Zaitsev M, Hennig J. Inversion recovery prepared turbo spin echo sequences with reduced SAR using smooth transitions between pseudo steady states. Magn Reson Med 2007;57:631–637.

28. Lukzen NN, Petrova MV, Koptyug IV, Savelov AA, Sagdeev RZ. The generating functions formalism for the analysis of spin response to the periodic trains of RF pulses. Echo sequences with arbitrary refocusing angles and resonance offsets. J Magn Reson 2009;196:164–169.

29. Busse RF, Hariharan H, Vu A, Brittain JH. Fast spin echo sequences with very long echo trains: design of variable refocusing flip angle schedules and generation of clinical T2 contrast. Magn Reson Med 2006;55:1030–1037.

30. Kiselev VG. Calculation of diffusion effect for arbitrary pulse sequences. J Magn Reson 2003;164:205–211.

31. Weigel M, Hennig J. Contrast behavior and relaxation effects of conventional and hyperecho-turbo spin echo sequences at 1.5 and 3T. Magn Reson Med 2006;55:826–835.

32. Carr HY. Steady-state free precession in nuclear magnetic resonance. Phys Rev 1958;112:1693.

33. Oppelt A, Graumann R, Barfuss H, Fischer H, Hartl W, Schajor W. FISP: Eine neue schnelle Pulssequenz fuer die Kernspintomographie. Electromedica 1986;54:15–18.

34. Zur Y, Wood ML, Neuringer LJ. Spoiling of transverse magnetization in steady-state sequences. Magn Reson Med 1991;21:251–263.

35. Hennig J, Hodapp M. Burst imaging. Magn Reson Mater Phys 1993;1:39–48.

36. Lowe IJ, Wysong RE. DANTE Ultrafast Imaging Sequence (DUFIS). J Magn Reson 1993;101:106–109.

37. Heid O, Deimling M, Huk WJ. Ultra-rapid gradient echo imaging. Magn Reson Med 1995;33:143–149.

38. Hennig J, Il'yasov KA, Weigel M. Imaging with positive T1-contrast using superstimulated echoes. Magn Reson Med 2012;68:1157–1165.

39. Busse RF, Brau AC, Vu A, et al. Effects of refocusing flip angle modulation and view ordering in 3D fast spin echo. Magn Reson Med 2008;60:640–649.

40. Weigel M, Hennig J. Development and optimization of T2 weighted methods with reduced RF power deposition (Hyperecho-TSE) for magnetic resonance imaging. Z Med Phys 2008;18:151–161.

41. Mugler JP, Bao S, Mulkern RV, et al. Optimized single-slab three-dimensional spin-echo MR imaging of the brain. Radiology 2000;216:891–899.

42. Mugler JP, Kiefer B, Brookeman JR. Three-dimensional T2-weighted imaging of the brain using very long spin-echo trains. In: Proceedings of the 8th Scientific Meeting of ISMRM, Denver, 2000. (abstract 687).

43. Bieri O, Ganter C, Welsch GH, Trattnig S, Mamisch TC, Scheffler K. Fast diffusion-weighted steady state free precession imaging of in vivo knee cartilage. Magn Reson Med 2012:691–700.

44. Lauterbur PC. Image formation by induced local interactions. Examples employing nuclear magnetic resonance. Nature 1973;242:190–191.

45. Mansfield P, Grannell PK. NMR diffraction in solids. J Phys C 1973;6:422.

46. Damadian R. Tumor detection by nuclear magnetic resonance. Science 1971;171:1151–1153.

47. Bernstein MA, King KF, Zhou XJ. Handbook of MRI pulse sequences. New York: Elsevier Academic Press; 2004.

48. Zur Y, Stokar S. A phase-cycling technique for cancelling spurious echoes in NMR imaging. J Magn Reson 1987;71:212–228.

49. Zur Y, Stokar S, Bendel P. An analysis of fast imaging sequences with steady-state transverse magnetization refocusing. Magn Reson Med 1988;6:175–193.

50. Bodenhausen G, Freeman R, Morris GA. A simple pulse sequence for selective excitation in Fourier transform NMR. J Magn Reson 1976;23:171–175.

51. Morris GA, Freeman R. Selective excitation in fourier transform nuclear magnetic resonance. J Magn Reson 1978;29:433–462.

52. Lee KJ, Zahneisen B, Hennig J, Weigel M, Leupold J. Multiplex RARE: a simultaneous multislice spin-echo sequence that fulfils CPMG conditions. Magn Reson Med 2010;64:299–305.

53. Freed DE, Scheven UM, Zielinski LJ, Sen PN, Hurlimann MD. Steady-state free precession experiments and exact treatment of diffusion in a uniform gradient. J Chem Phys 2001;115:4249–4258.

54. Freed DE, Hurlimann MD, Scheven UM. The equivalence between off-resonance and on-resonance pulse sequences and its application to steady-state free precession with diffusion in inhomogeneous fields. J Magn Reson 2003;162:328–335.

55. Rodriguez I, Perez de Alejo R, Ruiz-Cabello J. Pathway selection by pulsed field gradients. Magn Reson Med 2002;48:540–542.

56. Lebel RM, Wilman AH. Time-efficient fast spin echo imaging at 4.7 T with low refocusing angles. Magn Reson Med 2009;62:96–105.

57. Scheffler K, Heid O, Hennig J. Magnetization preparation during the steady state: fat-saturated 3D TrueFISP. Magn Reson Med 2001;45:1075–1080.

58. Weigel M, Hennig J. Diffusion sensitivity of turbo spin echo sequences. Magn Reson Med 2012;67:1528–1537.

59. Stocker T, Shah NJ. MP-SAGE: a new MP-RAGE sequence with enhanced SNR and CNR for brain imaging utilizing square-spiral phase encoding and variable flip angles. Magn Reson Med 2006;56:824–834.

60. Markl M, Leupold J. Gradient echo imaging. J Magn Reson Imaging 2012;35:1274–1289.

61. Hargreaves B. Rapid gradient-echo imaging. J Magn Reson Imaging 2012;36:1300–1313.

62. Bieri O, Scheffler K. Fundamentals of balanced steady state free precession MRI. J Magn Reson Imaging 2013;38:2–11.

63. Hurlimann MD. Diffusion and relaxation effects in general stray field NMR experiments. J Magn Reson 2001;148:367–378.

64. Song YQ, Hurlimann MD, Flaum C. A method for rapid characterization of diffusion. J Magn Reson 2003;161:222–233.

65. Carney CE, Wong ST, Patz S. Analytical solution and verification of diffusion effect in SSFP. Magn Reson Med 1991;19:240–246.

66. Le Bihan D, Mangin JF, Poupon C, et al. Diffusion tensor imaging: concepts and applications. J Magn Reson Imaging 2001;13:534–546.

67. Basser PJ, Mattiello J, LeBihan D. Estimation of the effective self-diffusion tensor from the NMR spin echo. J Magn Reson B 1994;103:247–254.

68. Bieri O, Ganter C, Welsch GH, Trattnig S, Mamisch TC, Scheffler K. Fast diffusion-weighted steady state free precession imaging of in vivo knee cartilage. Magn Reson Med 2012:691–700.

69. McNab JA, Miller KL. Steady-state diffusion-weighted imaging: theory, acquisition and analysis. NMR Biomed 2010;23:781–793.

70. Larson PE, Kerr AB, Reed GD, et al. Generating super stimulated-echoes in MRI and their application to hyperpolarized C-13 diffusion metabolic imaging. IEEE Trans Med Imaging 2012;31:265–275.

71. Malik SJ, Padormo F, Price AN, Hajnal JV. Spatially resolved extended phase graphs: modeling and design of multipulse sequences with parallel transmission. Magn Reson Med 2012;68:1481–1494.

72. Pauly J, Le Roux P, Nishimura D, Macovski A. Parameter relations for the Shinnar-Le Roux selective excitation pulse design algorithm. IEEE Trans Med Imaging 1991;10:53–65.

73. Leupold J, Hennig J, Scheffler K. Moment and direction of the spoiler gradient for effective artifact suppression in RF-spoiled gradient echo imaging. Magn Reson Med 2008;60:119–127.

74. Hennig J. Generalized MR interferography. Magn Reson Med 1990;16:390–402.

75. Hennig J, Scheffler K. Hyperechoes. Magn Reson Med 2001;46:6–12.